INRIA

INSTITUT NATIONAL DE RECHERCHE EN INFORMATIQUE ET EN AUTOMATIQUE

A numerical study on large-time asymptotics of the Lifshitz-Slyozov system

José Antonio Carrillo — Thierry Goudon

N° 4287

octobre 2001

THÈME 4

ISSN 0249-6399 ISRN INRIA/RR--4287--FR+ENG

INRIA
SOPHIA ANTIPOLIS

A numerical study on large-time asymptotics of the Lifshitz-Slyozov system

José Antonio Carrillo * , Thierry Goudon†

Thème 4 — Simulation et optimisation
de systèmes complexes
Projet Caiman

Rapport de recherche n° 4287 — octobre 2001 — 43 pages

Abstract: We numerically investigate the behaviour for long time of solutions of the Lifshitz-Slyozov system. In particular, we find this behaviour to crucially depend on the distribution of largest aggregates present in the solution.

Key-words: Lifschitz-Slyozov system, Coagulation-fragmentation models, Phase transition, WENO schemes

* Departamento de Matemática Aplicada, Universidad de Granada, E-18071 Granada, Spain, carrillo@ugr.es

† Labo. J.A. Dieudonné UMR 6621, Université Nice-Sophia Antipolis, Parc Valrose, F-06108 Nice cedex 02, France, et INRIA project CAIMAN, BP 93, 06902 Sophia Antipolis Cédex, France, goudon@math.unice.fr

Unité de recherche INRIA Sophia Antipolis
2004, route des Lucioles, BP 93, 06902 Sophia Antipolis Cedex (France)
Téléphone : +33 4 92 38 77 77 — Télécopie : +33 4 92 38 77 65

Une étude numérique des comportements en temps longs du système de Lifshitz-Slyozov

Résumé : Nous étudions le comportement en temps long de solutions du système de Lifshitz-Slyozov. En particulier, il apparaît que ce comportement dépend de manière cruciale de la distribution des aggrégats les plus gros présents dans la solution.

Mots-clés : système de Lifschitz-Slyozov, modèles de coagulation-fragmentation, transition de phase, schémas WENO

1 Introduction

We aim at investigating numerically the asymptotic behaviour of the solutions (c, f) of the following Lifshitz-Slyozov (LS) equations

$$\begin{cases} \dfrac{\partial f}{\partial t} + \dfrac{\partial}{\partial x}[(a(x)c(t) - b(x))f] = 0 \ \text{ in } \mathbb{R}_t^+ \times \mathbb{R}_x^+, \\ c(t) + \displaystyle\int_{\mathbb{R}^+} x f(t,x)\, dx = \rho > 0, \\ f_{|t=0} = f_0 \ \text{ in } \mathbb{R}_x^+, \qquad c_{|t=0} = c_0. \end{cases} \tag{1}$$

This equation has been introduced in [17] as a model for the formation of a new phase in solid solutions. It is intended to describe the later stages of formation of the new phase: there exists yet a non negligible number of precipitates having a supercritical size. In the earlier stages, fluctuations effects lead to the formation of these crystal germs. Here, the evolution of the precipitates is described through the density $f(t, x)$ of clusters having, at time t, the size $x \geq 0$. The dynamics is governed by a mechanism of removal from or addition to the clusters of free particles whose size is infinitely small compared to the size of the aggregates. These free particles are called "monomers", and their density at time t is denoted by $c(t)$. Note however that the model requires in these ordering properties that the size of the aggregates remains small compared to the average distance between clusters; consequently, encounters and coalescence effects are neglected in this approximation.

The quantity $V(t, x) = a(x)c(t) - b(x)$ is interpreted as the growth rate, at time t, for a cluster having size x. The given coefficients $a, b \geq 0$ are thus the rates at which monomers are added to or removed from the cluster, respectively. The first relation in (1) is a conservation law in the size space, whereas the second relation is a constraint which expresses the conservation of the total mass of the material within the solution. The crucial assumption on the coefficients is the existence, at any time t, of a unique critical size $x_{c(t)}$ which splits the size domain:

$$\begin{aligned} V(t,x) = a(x)c(t) - b(x) < 0, \quad &\text{for} \quad 0 \leq x < x_{c(t)}, \\ V(t,x) = a(x)c(t) - b(x) > 0, \quad &\text{for} \quad x > x_{c(t)}. \end{aligned}$$

Indeed, in deriving the rate growth one considers the energy balance for a macroparticle, viewed as isolated in a bath of monomers, to maintain its size. Then, there is a competition between surface effects which tend to reduce the energetic cost due to the formation of an interface with volume effects associated to the bulk free energy of the cluster. The former are the dominating effects for small clusters. Accordingly, the evolution of a $x-$cluster is determined by the ratio between the monomers concentration $c(t)$ and an equilibrium concentration $c_e(x)$ characterized by the size x. It appears that $c_e(x)$ is a decreasing function of the size: there is a energetic advantage for the small grains to dissolve and transfer their mass to the large clusters. This phenomenom is known as the Ostwald ripening, [19]:

large grains are growing at the expenses of the small ones. From a technical viewpoint, this physical feature also explains why no boundary condition is needed at $x = 0$: the rate of growth $V(t,x)$ for small grains is negative. If one considers, at least formally, the characteristic curves

$$\frac{d}{dt}X(t;s,x) = V(t,X(t;s,x)), \qquad X(s;s,x) = x$$

then, they are pointing outside the domain $(0,+\infty)$ when they reach the origin. Precise form of the coefficients depends on the mechanism of mass transfer; assuming it is driven by diffusion, [17] gives the following coefficients

$$a(x) = x^{1/3}, \qquad b(x) = 1.$$

The critical size is therefore $x_{c(t)} = c^{-3}(t)$ in this case. For details on the model, we refer of course to the original paper of Lifschitz-Slyozov [17], but one may also consult the classical reference [16] and the recent review of Sagalovich-Slyozov [23].

Mathematical results establishing existence-uniqueness of solutions for (1) have been obtained recently, by using various approaches: we refer to Niethammer-Pego [20], Collet-Goudon [7], Laurençot [13]... On the other hand, derivation of (1) from the discrete model of Becker-Döring, an infinite system of ode's describing earlier stages of the new phase formation (see [2]), is discussed by Penrose [22], Collet-Goudon-Poupaud-Vasseur [9]. However, the asymptotic behaviour of the solution of (1) is not yet well understood, in contrast with the situation concerning discrete models for which we refer to Ball-Carr-Penrose [1]. In their seminal paper [17], Lifshitz-Slyozov argue on physical grounds the following conjectures:

CLS1 The monomers concentration $c(t)$ decreases as time goes to infinity; precisely, c goes to 0 and behaves as $Kt^{-1/3}$, where K is a universal constant, independent on the initial state of the system.

CLS2 The total number of the agglomerates, that is

$$m_0(t) = \int_{\mathbb{R}^+} f(t,x)\,dx$$

behaves as Ct^{-1}, C depending on K and ρ, the total mass of the system.

CLS3 The mean radius

$$R_m(t) = \frac{1}{m_0(t)} \int_{\mathbb{R}^+} x^{1/3} f(t,x)\,dx$$

goes to infinity like $t^{1/3}/K$.

CLS4 The solution $f(t,x)$ tends to a universal asymptotic profile, independently on the shape of the initial data: from the initial state, it only depends on ρ as a scale parameter. Therefore, the solution forgets its initial shape.

A very few things are known on the question of the asymptotic behaviour of (1). In [10], it is proved, by using an entropy method, that $c(t)$ goes to 0 when a part of the support of the initial data f_0 is situated on the right of the initial critical point. But monotonicity is not obtained. On the other hand, while people generally believe the $t^{-1/3}$ law for $c(t)$ (first part of conjecture **CLS1**), which has been verified experimentally, the questions of uniqueness of the value of K, and uniqueness and stability of the final attractor have originated a controversial debate.

In particular, it is argued that the tail of the initial data and the largest particles might play a crucial role and modify the asymptotic profile, see for instance Brown [3], Meerson-Sasorov [18]. According to these arguments, the mathematical analysis performed by Carr-Penrose [4] and Niethammer-Pego [21] indicates that the asymptotic behaviour highly depends on the tip of the support of the initial data. Actually, they are concerned with a slightly modified model, the Lifshitz-Slyozov-Wagner equation, see [25]. However, this variant of (1) is interesting enough since, roughly speaking, it should be close to (1) when c has become small, see [14]. In particular, from [18], [21] one might conjecture that, starting from a compactly supported initial data with

$$f_0(x) \sim (x_s - x)^a \ , \ a > -1,$$

x_s being the endpoint of the support, the system cannot converge to the profile predicted by Lifshitz-Slyozov. Instead, one expects the convergence towards another profile, for a different value of K, defined by the value of the exponent a (a part of these statements have been rigorously obtained for the modified model in [21]). This fact complements conjecture **CLS4** since it seems that in [17] they are dealing with initial data having unbounded support.

The general conclusion of our numerical study is that the behaviour predicted by Lifshitz-Slyozov cannot be expected for any initial data. Some assumptions on the initial repartition of the aggregates in size seems necessary for c going to 0; and, then, the asymptotic state highly depends on the largest particles in the solutions. Actually, these results are in good agreement with the conjectures introduced in [18], [21].

The paper is organized as follows. In Section 2, we briefly recall some basic facts about equation (1). In Section 3, we introduce a scaled version of (1), which is appropriate to investigate the large time behaviour of the system. From the rescaled equation, we discuss the possible asymptotic states. Then, in Section 4, we describe in detail the results of our numerical investigation of (1). The final Section is devoted to comments and conclusions on the study.

2 Basic properties of LS

Let us start with some basic remarks. In the sequel, we use the characteristics associated to the growth rate, neglecting the technical difficulties caused by the blow up of the derivative at $x = 0$. As in [7], it allows us to write the solution as

$$f(t,x) = f_0(X(0;t,x)) \ J(0;t,x) \tag{2}$$

where $J(s;t,x) = D_x X(s;t,x)$. Based on the characteristic form, we conclude:

1. The zeroth order moment, interpreted as the total number of clusters in the solution, reads, by using characteristics,

$$\int_{\mathbb{R}^+} f(t,x)\,dx = \int_{X(0;t,0)}^{\infty} f_0(x)\,dx.$$

   As a consequence of $V(t,0) < 0$, we realize that $D_t X(0;t,0) > 0$. Therefore

$$m_0 : t \longmapsto \int_{\mathbb{R}^+} f(t,x)\,dx \text{ is a non increasing function of time.}$$

   The main effect of the equation is to "stretch" the initial data: it is expected that "mass goes to infinity", clusters in the solution having larger and larger size. From [17], it is expected that m_0 behaves as t^{-1}.

2. The time derivative of the monomer concentration, is given by

$$\frac{dc}{dt} = -\int_{\mathbb{R}^+} V(t,x) f(t,x)\,dx = -\int_0^{x_{c(t)}} V(t,x) f(t,x)\,dx - \int_{x_{c(t)}}^{\infty} V(t,x) f(t,x)\,dx.$$

   The first term is non negative, the second is non positive. Hence, there is a struggle between these terms, depending on the repartition of the clusters in size to determine the variation of $c(t)$.

3. It can be shown that $c(t) > 0$ for any time t. Next, if the initial data f_0 has its support in $[0, x_s]$; then, by using the formula (2), we realize that the support of the solution is contained in $[0, X(t;0,x_s)]$. In particular, for $x_s < \infty$, the support of the solution remains bounded by $X(t,0,x_s) < \infty$. If initially the endpoint x_s of the support of the initial data satisfy $x_s > x_{c_0}$; then the critical size cannot reach the end of the support: $X(t;0,x_s) - x_{c(t)} > 0$ (see [10]).

4. According to [10], we expect that the total number of clusters $m_0(t)$ goes to 0 while the monomers concentration either tends to 0 or ρ. In particular, if there exists $\delta > 0$ such that $\mathrm{supp}(f_0) \cap [x_{c_0} + \delta, \infty[\neq \emptyset$, then $c(t) \to 0$. It is conjectured, for an initial data having its support in $[0, x_{c_0}]$, that the two behaviours: $c(t)$ goes to 0 or to ρ, are possible, depending crucially on the initial repartition of mass in the interval. We will see numerically that the two behaviours are indeed possible (see figures 7 and 8 below).

It is also worth saying some words on a variant of equation (1) which is commonly used. The Lifshitz-Slyozov-Wagner equation deals with a situation where c has reached indeed an equilibrium: it is small enough to be neglected in the mass conservation relation, which becomes

$$\int_{\mathbb{R}^+} x f(t,x)\,dx = \rho$$

i.e. a constraint on the first moment. However, we keep the c in the definition of the growth rate and the evolution equation still reads

$$\frac{\partial f}{\partial t} + \frac{\partial}{\partial x}[(a(x)c(t) - b(x))f] = 0$$

Integrating the equation after multiplication by x, and taking into account the constraint, one sees that c should satisfy

$$c(t) = \int_{\mathbb{R}^+} b(x)f(t,x)\,dx \left(\int_{\mathbb{R}^+} a(x)f(t,x)\,dx\right)^{-1}.$$

For the coefficients of [17], we recover

$$c(t) = \int_{\mathbb{R}^+} f(t,x)\,dx \left(\int_{\mathbb{R}^+} x^{1/3}f(t,x)\,dx\right)^{-1} = \frac{1}{R_m(t)},$$

i.e. the inverse of the mean radius of the agglomerates. Summarizing, the Lifshitz-Slyozov-Wagner (LSW) problem is to solve

$$\begin{cases} \dfrac{\partial f}{\partial t} + \dfrac{\partial}{\partial x}[(a(x)c(t) - b(x))f] = 0 \ \text{ in } \mathbb{R}_t^+ \times \mathbb{R}_x^+, \\ \\ c(t) = \displaystyle\int_{\mathbb{R}^+} b(x)f(t,x)\,dx \left(\int_{\mathbb{R}^+} a(x)f(t,x)\,dx\right)^{-1} \\ \\ f_{|t=0} = f_0 \ \text{ in } \mathbb{R}_x^+, \qquad c_{|t=0} = c_0. \end{cases} \tag{3}$$

It can be proved that the LSW equation (3) can be obtained from the LS one (1) by an asymptotic argument; see [14]. This is the model dealt with in [21] and [4] (the last one with the simplification $a(x) = x$, $b(x) = 1$).

3 Rescaled equation, and asymptotic profiles

In order to investigate the large time behaviour, Lifshitz-Slyozov make use of a scaling involving the critical size in the definition of the new time and space variables. However, monotonicity of $t \mapsto c(t)$ is not guaranteed at all (on the contrary, numerical simulations show that, especially at earlier stages, this function is not monotone, see [6] and Section 4), so that the change of variables in [17] does not make clearly sense. On the other hand, one expects that $c(t)$ behaves for large time as $Kt^{-1/3}$, thus the critical size $x_c(t)$ behaves as t/K^3. This behaviour is revealed by the numerical simulations, as we shall see in next section. This motivates the introduction of the following scaling:

$$\begin{cases} f(t,x) = \dfrac{1}{(1+t)^2} g\left(\ln(1+t), \dfrac{x}{1+t}\right), \\ \tau = \ln(1+t), \qquad y = \frac{x}{1+t}. \end{cases}$$

Roughly speaking, we replace x_c in the scaling of [17] by the monotone function $(1+t)$. We set

$$d(\ln(1+t)) = (1+t)^{1/3}c(t), \qquad w(\tau, y) = y^{1/3}d(\tau) - 1 - y.$$

A short computation leads to the following rescaled form of (1)

$$\left\{ \begin{array}{l} \dfrac{\partial g}{\partial \tau} + \dfrac{\partial}{\partial y}[w(\tau,y)g] = g, \\ d(\tau)e^{-\tau/3} + \displaystyle\int_{\mathbb{R}^+} yg(\tau,y)\,dy = \rho. \end{array} \right.$$

Based on the analysis of [17], confirmed on this aspect by the numerical tests in section 4, one expect that $c(t)t^{1/3}$ tends to some constant $K > 0$, i.e.

$$\lim_{\tau\to\infty} d(\tau) = K.$$

Accordingly, $d(\tau)e^{-\tau/3} \sim Ke^{-\tau/3}$ is negligible for large τ. Similarly, $w(\tau, y)$ looks like $w_K(y) = y^{1/3}K - 1 - y$. Thus, one is led to the following limit equation

$$\left\{ \begin{array}{l} \dfrac{\partial g}{\partial \tau} + \dfrac{\partial}{\partial y}[w_K(y)g] = g, \\ \displaystyle\int_{\mathbb{R}^+} yg(\tau,y)\,dy = \rho \end{array} \right. \tag{4}$$

Notice that, from previous equation and the constraint on the first moment of g, K is equal to the inverse of the mean radius

$$K = \int_{\mathbb{R}^+} g\,dy \left(\int_{\mathbb{R}^+} y^{1/3} g\,dy \right)^{-1}.$$

To go further, one needs to discuss some basic properties of the asymptotic growth rate $w_K(y) = W_K(y^{1/3})$, where W_K is the simple polynomial $W_K(z) = Kz - 1 - z^3$. We shall obtain a familly of possible asymptotic profiles, parameterized by K. We remark that W_K is concave on $(0, +\infty)$ and reaches its maximum at $z = \sqrt{K/3}$. We have, for $z \geq 0$,

$$W_K(z) \leq W_K^{max} = K(K/3)^{1/2} - 1 - (K/3)^{3/2} = 2(K/3)^{3/2} - 1.$$

Next, remark that W_K^{max} is an increasing function of K, from $(0, +\infty)$ to $(-1, +\infty)$, which vanishes at the critical value

$$K_{\text{crit}} = 3/2^{2/3}.$$

Therefore, we distinguish three cases:

a) $K < K_{\text{crit}}$: W_K has no positive roots, $W_K(z) \leq W_K^{max} < 0$ for $z \geq 0$.

b) $K > K_{\text{crit}}$: W_K has two distinct positive roots, z_0, z_+ (and a negative root z_-), and we have $W_K(z) \leq 0$ for $0 \leq z \leq z_0$ or $z \geq z_+$, and $W_K(z) \geq 0$ for $z_0 \leq z \leq z_+$. We will denote by y_-, y_+ and y_0 the correponding values for $w_K(y)$, i.e. $y_i = z_i^3$ for $i \in \{-, 0, +\}$.

c) $K = K_{\rm crit}$: $\sqrt{K_{\rm crit}/3} = 2^{-1/3}$ is a double root and $W_K(z) \le 0$ for $z \ge 0$.

Let us now look at the stationary solution M_K of (4)

$$\partial_y(w_K(y)M_K) = M_K \qquad \text{for } y \ge 0.$$

At least formally (up to the first positive zero $y_0 = z_0^3$ of w_K) we can write

$$M_K(y) = \frac{-1}{w_K(y)} \exp\left(\int_0^y \frac{d\sigma}{w_K(\sigma)}\right) = -\frac{d}{dy}\left[\exp\left(\int_0^y \frac{d\sigma}{w_K(\sigma)}\right)\right].$$

Furthermore, for such a solution to be admissible, it should satisfy the integrability condition $yM_K(y) \in L^1(\mathbb{R}^+)$.

We shall see that the subcritical case is unphysical; while for $K \ge K_{\rm crit}$, the value of K can be related, roughly speaking, to the behaviour of the stationary solution at the end of its support.

Proposition 3.1 *For $K < K_{\rm crit}$, there is no admissible stationary solution. For $K = K_{\rm crit}$, one obtains the Lifshitz-Slyozov profile*

$$M_{\rm crit}(y) = \frac{\exp\Big(-\dfrac{(2y)^{1/3}}{1-(2y)^{1/3}}\Big)}{(1-(2y)^{1/3})^{11/3}\ (1+\frac{1}{2}(2y)^{1/3})^{7/3}}, \tag{5}$$

for $0 \le y \le y_0 = 1/2$, and 0 otherwise. For $K > K_{\rm crit}$, one has

$$M_K(y) = (y_0 y_- y_+)^{1/3}\ \frac{\big(1-(y/y_0)^{1/3}\big)^{p-1}}{\big(1-(y/y_-)^{1/3}\big)^{1-q}\ \big(1-(y/y_+)^{1/3}\big)^{1-r}}, \tag{6}$$

for $0 \le y \le y_0$, and 0 otherwise, where the exponents $p \ge 0$, q, r depends on K. In particular, p and K are related by

$$K = \frac{3(p+1)}{(2p+3)^{2/3}\ p^{1/3}}. \tag{7}$$

Proof. The integrability requirement excludes the subcritical case $K < K_{\rm crit}$: we shall show that the first moment blows up. Indeed, for $K < K_{\rm crit}$, $\sigma \mapsto w_K(\sigma)^{-1}$ is defined on the whole interval $(0, +\infty)$, and we remark that, for any $y \ge 0$,

$$\begin{aligned}(1+y)\exp\left(\int_0^y \frac{d\sigma}{w_K(\sigma)}\right) &= \exp\left(\int_0^y \frac{d\sigma}{w_K(\sigma)} + \int_0^y \frac{d\sigma}{1+\sigma}\right)\\ &= \exp\left(\int_0^y \frac{K\ \sigma^{1/3}\,d\sigma}{(1+\sigma)(K\sigma^{1/3}-1-\sigma)}\right).\end{aligned}$$

The integrand is nonpositive and behaves for large σ's as $-K\sigma^{-5/3}$ which is integrable at infinity. It follows that

$$\lim_{y\to\infty}(1+y)\exp\left(\int_0^y \frac{d\sigma}{w_K(\sigma)}\right) = \ell > 0.$$

In particular, for $y \geq Y$ large enough, we have $(1+y)\exp(\int_0^y \frac{d\sigma}{w_K(\sigma)}) \geq \ell/2 > 0$. Since $-y/w_K(y) \to 1$ as $y \to \infty$, we deduce that

$$yM_K(y) = \frac{y}{-w_K(y)}\,(1+y)\exp\left(\int_0^y \frac{d\sigma}{w_K(\sigma)}\right)\,\frac{1}{1+y} \geq \frac{\ell}{4}\,\frac{1}{1+y},$$

holds for $y \geq Y$ large enough. Consequently $yM_K(y) \notin L^1(\mathbb{R}^+)$ for $K < K_{\rm crit}$. Lifshitz-Slyozov also exclude in their analysis the case $K > K_{\rm crit}$; however, this is far from clear, in particular when dealing with compactly supported initial data, see [4], [21], [18].

Let us now look at the critical case $K = K_{\rm crit} = 3/2^{2/3}$. We can rewrite $W_{\rm crit}(z) = (z - 2^{-1/3})^2(z + 2^{2/3})$. Accordingly, we get for $0 \leq y \leq 1/2$

$$\begin{aligned}
\int_0^y \frac{d\sigma}{w_{K_{\rm crit}}(\sigma)} &= \int_0^{y^{1/3}} \frac{3z^2\,dz}{W_{K_{\rm crit}}(z)} \\
&= \int_0^{y^{1/3}} \Big(\frac{-5/3}{z-2^{-1/3}} - \frac{2^{1/3}}{(z-2^{-1/3})^2} - \frac{4/3}{z+2^{2/3}}\Big)\,dz \\
&= 1 + \frac{1}{(2y)^{1/3}-1} + \ln\left(\frac{\big(1-(2y)^{1/3}\big)^{-5/3}}{\big(1+(y/4)^{1/3}\big)^{4/3}}\right),
\end{aligned}$$

which yields the announced formula (5) for $0 \leq y \leq y_0 = 1/2$.

We turn to the supercritical case $K > K_{\rm crit}$. The polynomial W_K has three distinct roots denoted by

$$z_- < 0 < z_0 < \sqrt{K/3} < z_+.$$

Let us write $z_\pm$ in terms of the first positive root z_0 as follows

$$\left\{\begin{array}{l} W_K(z) = -(z-z_0)(z^2+z_0z-(K-z_0^2)) = -(z-z_0)(z-z_+)(z-z_-) \\ z_\pm = \dfrac{1}{2}(z_0 \pm \sqrt{4K-3z_0^2}). \end{array}\right.$$

We aim at computing

$$\begin{aligned}
\int_0^y \frac{d\sigma}{w_K(\sigma)} &= \int_0^{y^{1/3}} \frac{-3z^2\,dz}{(z-z_0)(z-z_+)(z-z_-)} \\
&= \int_0^{y^{1/3}} \Big(\frac{p}{z-z_0} + \frac{q}{z-z_+} + \frac{r}{z-z_-}\Big)\,dz
\end{aligned}$$

where we check that

$$p = \frac{3z_0^2}{(z_0 - z_-)(z_+ - z_0)}, \quad q = \frac{-3z_-^2}{(z_0 - z_-)(z_+ - z_-)}, \quad r = \frac{-3z_+^2}{(z_+ - z_0)(z_+ - z_-)}.$$

For convenience, let us set

$$\kappa = \frac{K}{3z_0^2} \geq 1, \qquad \alpha = \frac{1}{2}(-1 + \sqrt{3}\sqrt{4\kappa - 1}),$$

so that

$$z_+ = \alpha z_0, \quad z_- = -z_0 - z_+ = -z_0(1 + \alpha),$$

and

$$p = \frac{3}{(2+\alpha)(\alpha - 1)} = \frac{1}{\kappa - 1} \geq 1, \quad q = \frac{-3\alpha^2}{(2\alpha+1)(\alpha - 1)}, \quad r = \frac{-3(\alpha+1)^2}{(2+\alpha)(2\alpha+1)}.$$

Hence, we get

$$\int_0^y \frac{d\sigma}{w_K(\sigma)} = \ln\left\{ \left(1 - (y/y_0)^{1/3}\right)^p \left(1 - (y/y_-)^{1/3}\right)^q \left(1 - (y/y_+)^{1/3}\right)^r \right\}$$

which yields the announced formula (6).

The behaviour at the endpoint y_0 is determined by the exponent $p - 1$. Recall this quantity is related to the value of

$$K = \lim_{t \to \infty} c(t) t^{1/3} = \lim_{\tau \to \infty} d(\tau)$$

by the relation

$$p = \frac{1}{\kappa - 1}, \qquad \kappa = \frac{K}{3z_0^2}$$

where z_0 is the first positive root of W_K i.e. $W_K(z_0) = 0 = Kz_0 - 1 - z_0^3$. This allows us to express K as a function of the exponent p as in the relation (7).

For $K \geq K_{\text{crit}}$, we have computed the stationary solution M_K up to the first positive root y_0 of w_K, where it vanishes. It remains to check that the integrability condition implies that M_K should be extended by 0 for $y \geq y_0$.

Note that M_{crit} is C^∞ at the tip of its support y_0, while the stationary solutions M_K are less regular as K increases, i.e. p tends to 0 (see fig. 1 for a comparizon of the graphs). $\diamond$

Remark 3.1 *For $p \geq 2$, M_K and M_K' vanish at the end of their support. For $p = 2$, M_K vanishes but M_K' is a positive constant as $y \to y_0$ (it behaves like a triangle function). For $1 < p < 2$, M_K vanishes and M_K' blows up as $y \to y_0$. For $p = 1$, M_K behaves like a step function. For $0 < p < 1$, M_K and M_K' blow up as $y \to y_0$ with an integrable singularity. For $p \to 0$, M_K looks like a Dirac function at y_0.*

Let us go back to the rescaled equation (4) when d has reached its equilibrium value. Set $g(\tau,y)=h(\tau,y)M_K(y)$. It follows that

$$\partial_\tau h + w_K(y)\partial_y h = 0.$$

Hence, integrating along the associated characteristics, we can write

$$h(\tau,y)=\chi(\tau-\Phi_K(y)),\qquad \Phi_K(y)=\int_0^y \frac{d\sigma}{w_K(\sigma)}.$$

Furthermore, the mass conservation yields

$$\int_{\mathbb{R}^+} yh(\tau,y)M_K(y)\,dy=\rho=\int_{\mathbb{R}^+} y\ \chi(\tau-\Phi_K(y))\ M_K(y)\,dy.$$

With the change of variables $z=\tau-\Phi_K(y)\geq 0$, this can be rewritten as

$$\rho=\int_\tau^\infty \Phi_K^{-1}(\tau-z)e^{\tau-z}\ \chi(z)\,dz,$$

where $\Phi_K^{-1}:(-\infty,0]\to[0,y_0)$ is the inverse of the decreasing function $\Phi_K:[0,y_0)\to(-\infty,0]$. An obvious solution of this equation is given by $\chi(y)=A$ constant, determined by the relation

$$A=\rho\left(\int_{\mathbb{R}^+} yM_K(y)\,dy\right)^{-1}.$$

It yields

$$f(t,x)=\frac{1}{(1+t)^2}g\left(\ln(1+t),\frac{x}{1+t}\right)\sim\frac{A}{(1+t)^2}\ M_K\left(\frac{x}{1+t}\right)$$

for large time. The zeroth order moment of f, i.e. the total number of clusters, behaves as

$$m_0(t)=\int_{\mathbb{R}^+} f(t,x)\,dx\sim\frac{A}{1+t}\int_{\mathbb{R}^+} M_K\left(\frac{x}{1+t}\right)\frac{dx}{1+t}\sim\frac{A}{t}\ \int_{\mathbb{R}^+} M_K(y)dy$$

In view of the discussion above and the results for the LSW and similar problems in [18], [4], [21], one might expect the following conjecture for the LS system. If the initial data is compactly supported in $[0,x_s]$, with $f_0(x)\sim C(x_s-x)^{p-1}$ when $x\to x_s$, then the solution satisfies

$$f(t,x)\sim\frac{A}{(1+t)^2}\ M_K\left(\frac{x}{1+t}\right) \tag{8}$$

where K is associated to p by (7). If f_0 has unbounded support, the conjecture is

$$f(t,x)\sim\frac{A}{(1+t)^2}\ M_{\text{crit}}\left(\frac{x}{1+t}\right), \tag{9}$$

i.e., f is described by the LS profile. This conjecture implies that **CLS2-CLS3** hold with the corresponding value for K.

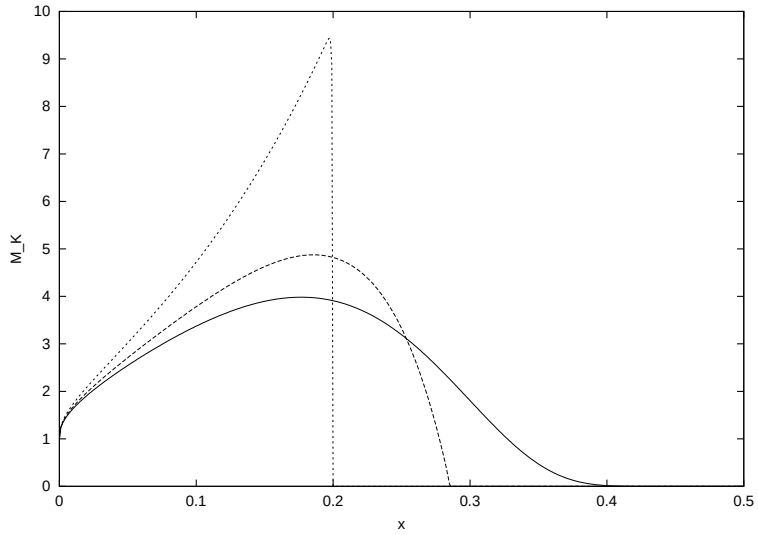

Figure 1: Comparisons of the stationary solutions M_K profiles for the discontinuous case $p = 1$, the corner case $p = 2$ and the smooth case $p = \infty$ (LS profile).

4 Numerical simulation of LS

We wish to investigate numerically the question of the asymptotic behaviour of solutions of (1). We have seen the possibility of having different asymptotic states depending on the behaviour near the tip of the support in previous section. This is the main point we would like to validate numerically.

Is the smooth stationary state M_{crit} the universal long-time profile for the LS system? Are there any other initial data that leads to the non-smooth selfsimilar profiles M_K for $K > K_{\text{crit}}$? The LS conjecture **CLS4** asserts that the answer to the first question is affirmative. However, we will show by a carefully constructed numerical scheme that in fact, the second answer is affirmative and the LS conjecture **CLS4** in its full generality is not true. Nevertheless, non compactly supported initial data and smooth compactly supported initial data lead asymptotically to the LS profile, based on the numerics. The rigorous proof of these results was achieved in part for the modified LS equation in [21] but for the real LS system (1) this proof is still lacking.

This section is divided into two subsections: in the first one we describe the numerical scheme used to discretize (1), the second one is devoted to the numerical simulation results in which the previous assertions are based and their discussion.

4.1 Numerical method

We treat the evolution equation

$$\frac{\partial f}{\partial t} + \frac{\partial}{\partial x}[V(t,x)f] = 0 \tag{10}$$

as a linear one-dimensional advection equation with time and position dependent advection function $V(t,x) = a(x)c(t) - b(x)$, for a given known monomer concentration $c(t)$. In order to solve numerically such linear advection equation we can use any standard numerical scheme [15, 24] considered for nonlinear one-dimensional and multi-dimensional conservation laws. In order to choose a suitable scheme for solving (10), we have to take into consideration several facts:

1. One of the effects over the solution we observe is the stretching of the support of the solution. Thus, one needs to deal with a large domain of computation.

2. The expected asymptotic profile depends crucially on the behaviour of the data at the end of the support; therefore, smoothing effects induced by the numerical scheme can modify the final profile. As a consequence, one should choose the least dissipative choice among all the possible numerical schemes. Intuitively, the LS evolution acts in this way: zoom the tip of the support, cut the rest, strecht it and multiply by an amplification factor. Thus, smoothing effects done by the numerical approximations are doomed to be amplified during the evolution. That is the main reason we need the least possible dissipative numerical scheme.

3. High order accuracy for the solution in space is desirable since we expect the solution to be very smooth outside possibly the tip of the support. If we have initial solutions with jumps or corner discontinuities at the tip of the support, we expect them to propagate in time, so we also would need a numerical scheme that preserves shocks or corner discontinuities with a good accuracy, if they appear (see figures 1, 2).

4. High order in time, TVD discretizations and stability in time are of paramount importance to obtain meaningful numerical results after so many time iterations.

Based on these facts, we decide to choose a standard finite volume solver of the linear advection equation (10) with Godunov flux as monotone flux. The choice of Godunov flux is due to the fact that is the least dissipative (less smearing of jumps or corners) with respect to other standard fluxes: Lax-Friedrichs, Engquist-Osher,...

In the reconstruction part we want to achieve high order in smooth parts of the solution (that for (1) is always the case except possibly at the tip of the support) and also good accuracy at shocks (jumps) or corners, if they appear initially. Therefore, we choose WENO reconstruction with 5 points wich gives you fifth-order spatial accuracy for smooth solutions. We refer to [12, 24] for the details of the numerical method. This method has been tested throughly and it has been shown to be very robust and to produce meaningful results for

complicated non linear systems of conservation laws in fluid dynamics, semiconductors, Hamilton-Jacobi equations,... (see [24, 5]).

We solve in time by means of an explicit 3rd-order TVD Runge-Kutta method introducedby C. W. Shu [24] that enjoys the needed features of stability, high order and TVD character. CFL condition is verified at each time step to ensure numerical stability. The algebraic condition

$$c(t) + \int_{\mathbb{R}+} x f(t,x)\, dx = \rho > 0,$$

is used to determine the monomer concentration $c(t)$ at the begining of each time-step to compute the fluxes correctly.

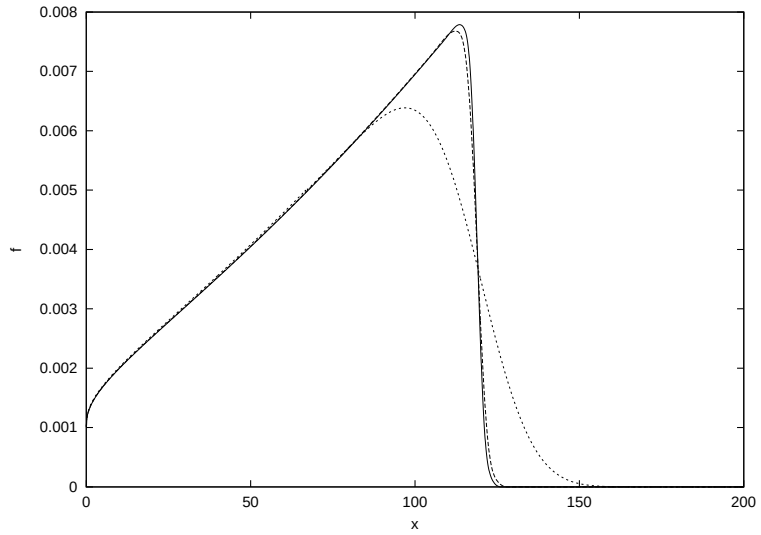

Figure 2: Comparisons of the numerical solutions for a step-like function initial data ($f = 0.1$ for $10 \leq x \leq 30$ and 0 outside) using finite volume Godunov-WENO, finite volume Lax-Friedrichs-WENO and upwinding finite difference method. The results given by Godunov-WENO are the least smeared, the upwinding results are the smoother ones.

In figure 2 we show the solution of this system for a step-like initial data after 200 units of time by using the finite volume Godunov-WENO, finite volume Lax-Friedrichs-WENO and the simple upwinding finite differences method (finite volume Godunov-first order reconstruction). Experts in numerical schemes for conservation laws can recognize easily that the simple upwinding method gives very smeared non realistic solutions for the linear advection equation with a step function as an initial data [15].

In fact the results of simulations for this system using the upwinding method were reported in [6]. They asserted that the LS conjecture was true by using different shapes of initial data, all of them with empty zero level set (non compact support). The smearing

caused by the use of the simple upwinding method disables the possibility of finding any other possible behaviour. In fact, as figure 2 shows, the use of this method for a step-like initial data can lead you to a completely wrong conclusion asserting the convergence towards the smooth self similar solution and therefore that the LS profile is the universal asymptotic behaviour for any initial data. This method is not at all suitable for controlling the behaviour at the tip of the support. Moreover, they obtain limiting critical values $K_{\rm crit}$ with a error of $5-20\%$.

Finally, let just mention that the numerical simulation of the rescaled equation

$$\begin{cases} \partial_\tau g + \partial_y(w(\tau,y)g) = g, \\ \\ d(\tau)e^{-\tau/3} + \displaystyle\int_{\mathbb{R}^+} yg(\tau,y)\,dy = \rho. \end{cases}$$

is done following the same lines as above. The main advantage of this rescaled form is that we can work in a much smaller x-interval. Despite of this fact, the CFL condition for the rescaled equation is much more restrictive (stiffer problem) than for the original LS system. Therefore, computational times are almost identical for both problems, but the rescaled system allows us to explore easier the later stages of the evolution. Also, the modified LSW system is solved in an analogous way to the LS system.

4.2 Simulation results

4.2.1 Validation of the code

First, we validate our code by comparing simulation results to explicit solutions. Explicit solutions were obtained in [7] for very simple coefficients without critical size. In particular, the simplest case is $a(x) = ax$, $b(x) = bx$, with $a, b > 0$ constants, where the solution is exactly known

$$f(t,x) = \beta(t) f_0(\beta(t)x),$$

with

$$\beta(t) = \begin{cases} \dfrac{(ac_0 - b)\exp((b-a\rho)t) + a(\rho - c_0)}{a\rho - b}, & \text{for } a\rho - b \neq 0, \\ \\ \beta(t) = 1 + a(\rho - c_0)t, & \text{for } a\rho - b = 0, \end{cases}$$

whereas

$$c(t) = \begin{cases} \dfrac{\rho(ac_0 - b)\exp((b-a\rho)t) + b(\rho - c_0)}{(ac_0 - b)\exp((b-a\rho)t) + a(\rho - c_0)}, & \text{for } a\rho - b \neq 0, \\ \\ \dfrac{c_0 + \rho(\rho - c_0)at}{1 + (\rho - c_0)at}, & \text{for } a\rho - b = 0, \end{cases}$$

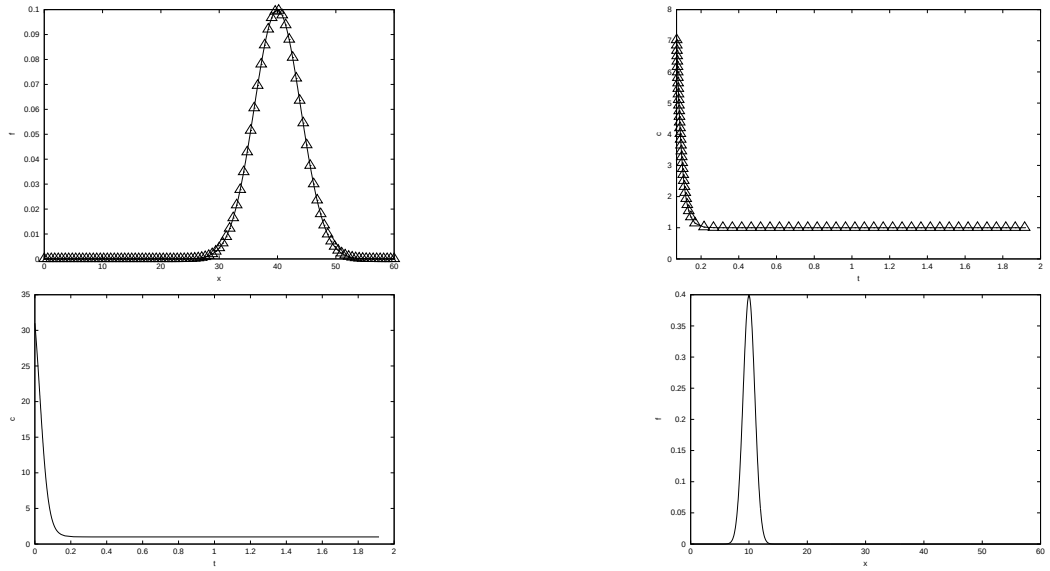

Figure 3: Test1: top left: final computed solution (solid line) versus exact explicit stationary (triangles); top right: $c(t)$ for the computed solution (solid line) versus the exact explicit evolution of concentration of monomers (triangles); bottom left: $c(t)$; bottom right: initial data.

Then, the asymptotic behaviour is obtained easily, depending on the over or undersatured nature of the initial data. Precisely, one has:

If $\rho < b/a$, then $c(t) \to \rho$ and

$$f(t,x) \sim \frac{b/a - c_0}{b/a - \rho}\ e^{(b/a-\rho)at}\ f_0\left(\frac{b/a - c_0}{b/a - \rho} e^{(b/a-\rho)at}\, x\right),$$

If $\rho > b/a$, then $c(t) \to b/a$ and

$$f(t,x) \to f_\infty(x) = \frac{\rho - c_0}{\rho - b/a}\ f_0\left(\frac{\rho - c_0}{\rho - b/a}\, x\right).$$

We use this simple case to validate the performance of the scheme. The first test (Test 1) corresponds to $a = b = 1$, $\rho = 41 > b/a$, $c_0 = 31$. The initial data, represented in fig. 3 bottom right, is a Maxwellian

$$f_0(x) = \frac{m}{\sqrt{2\pi}}\ \exp\left(-\frac{(x-10)^2}{2}\right).$$

Figure 3 shows an exact agreement of the computed solution with the exact behaviour given

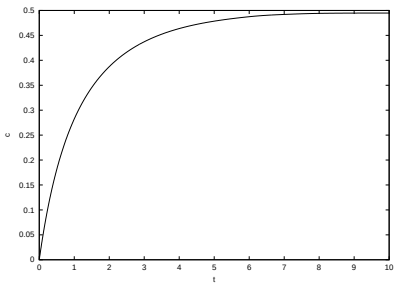

Figure 4: Test2: $c(t)$ for the computed solution.

by

$$c(t) = \frac{40 \times 30 \times e^{-40t} + 10}{30 \times e^{-40t} + 10} \to 1 = b/a,$$

and $f(t,x) \sim \frac{1}{4} f_0(\frac{x}{4})$ as $t \to \infty$. The second test (Test 2) is $a = b = 1$, $\rho = .5 < b/a$, $c_0 << 1$ for which we recover the expected behaviour $c(t) \sim .5$ and

$$f(t,x) \sim 2e^{t/2} f_0(e^{t/2}x) \sim \frac{2m}{\sqrt{2\pi e^{-t}}}\ \exp\big(-\frac{(x - 10e^{-t/2})^2}{2e^{-t}}\big) \sim 2m\ \delta_{x=0},$$

as $t \to \infty$. The monomer concentration evolution is given in Figure 4.

4.2.2 Simulations on the LS equation

Once we have validated our code we take the true LS system with the coefficients of [17], $a(x) = x^{1/3}$, $b(x) = 1$. We first, choose as initial data f_0 a Maxwellian centered on x_o comparable to, or larger than, the critical size. This is the situation in Theorem 1 [10] where $c(t)$ goes to 0 as $t \to \infty$. Precisely, we set for this run: $\rho = 41$, $c_0 = 1$ (thus $x_{c_0} = 1$) and the Maxwellian

$$f_0(x) = \frac{m}{\sqrt{2\pi}} \exp\left(-\frac{(x-10)^2}{2}\right).$$

as initial data (see figure 3 bottom right).

After 2000 units of time, one observes (see Figures 5 and 6):

1. A metastability region for the concentration of monomers before $c(t)$ decreases.
2. A good agreement with the $t^{-1/3}$ law, as shown in the graph of $K(t) = t^{1/3}c(t)$. We can observe that it converges very quickly towards values very close to $K_{\text{crit}} = 1.88988$, and after $K(t)$ changes very slowly decreasing their value until reaching $K(2000) = 1.8657$. We may run the code further to observe that there after $K(t)$ starts to increase slowly aproaching the critical value $K_{\text{crit}} = 1.88988$, but we will see this fact later in the rescaled equation.
3. m_0 decreases after the metastability region, in good agreement with the t^{-1} law.
4. The evolution of this solution is summarized in Figure 6 which shows the solution $f(t,x)$ each 250 units of time. We can see clearly the stretching of the support and the convergence towards the shape of the LS profile. In figure 5 bottom right we have plotted the final solution after 2000 units of time versus the LS profile in the selfsimilar variables corresponding to this time and to this value of ρ according to formula (9).

Next, we choose a very small c_0, thus a very large critical size. The initial data f_0 is a Maxwellian centered on x_0 much smaller than the critical size, with a small variance, so that it is almost a compactly supported data, with support to the left of the critical size. Then, one verifies that c goes to ρ. This is illustrated with the data: $c_0 = 7.10^{-2}$, $\rho = .2$ and f_0 is a Maxwellian centered at 0, with mass .1 and variance 10, given in figure 7 top left. After 45 units of time, one sees that c goes very close to ρ (see figure 7 top right) and the final profile $f(t,x)$ is almost zero (see figure 7 bottom).

However, this behaviour is very sensitive to the initial data, it changes drastically if the initial critical size is reduced or if one increases the "support" of f_0 (for instance, changing the variance of the Maxwellian). We consider the same test as before changing $c_0 = .5$, $\rho = 2$, variance of f_0 equals .01 (see figure 8 top left). Then, c starts increasing, reaching values very close to ρ, but the evolution changes and finally it decreases to 0, as illustrated by figure 7 top right. We then recover a good agreement again with the $t^{-1/3}$ law, see figure 8 bottom left. Figure 8 bottom right gives the final solution f, after 100 units of time.

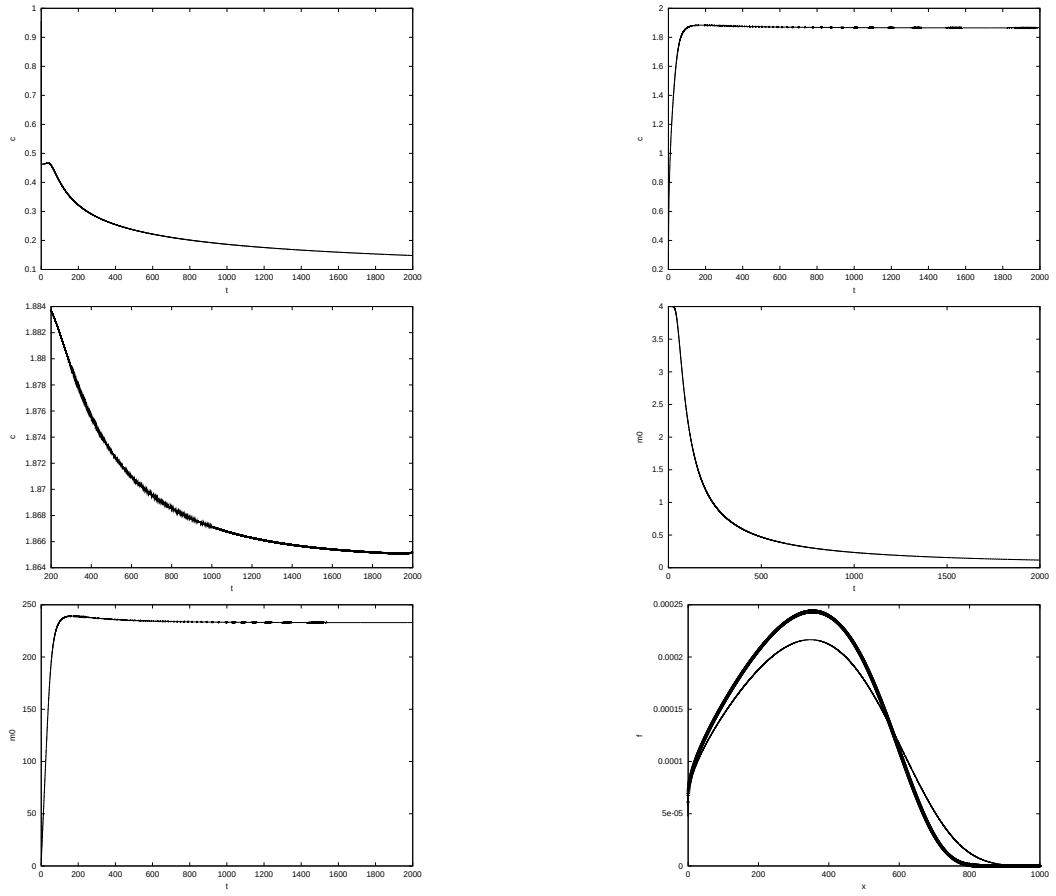

Figure 5: Maxwellian initial data for the LS system ($c(t) \to 0$): top left: $c(t)$; top right: $t^{1/3}c(t)$; middle left: zoom of $t^{1/3}c(t)$; middle right: $m_0(t)$; bottom left: $tm_0(t)$; bottom right: final result (solid line) versus the corresponding LS profile (thicker solid line).

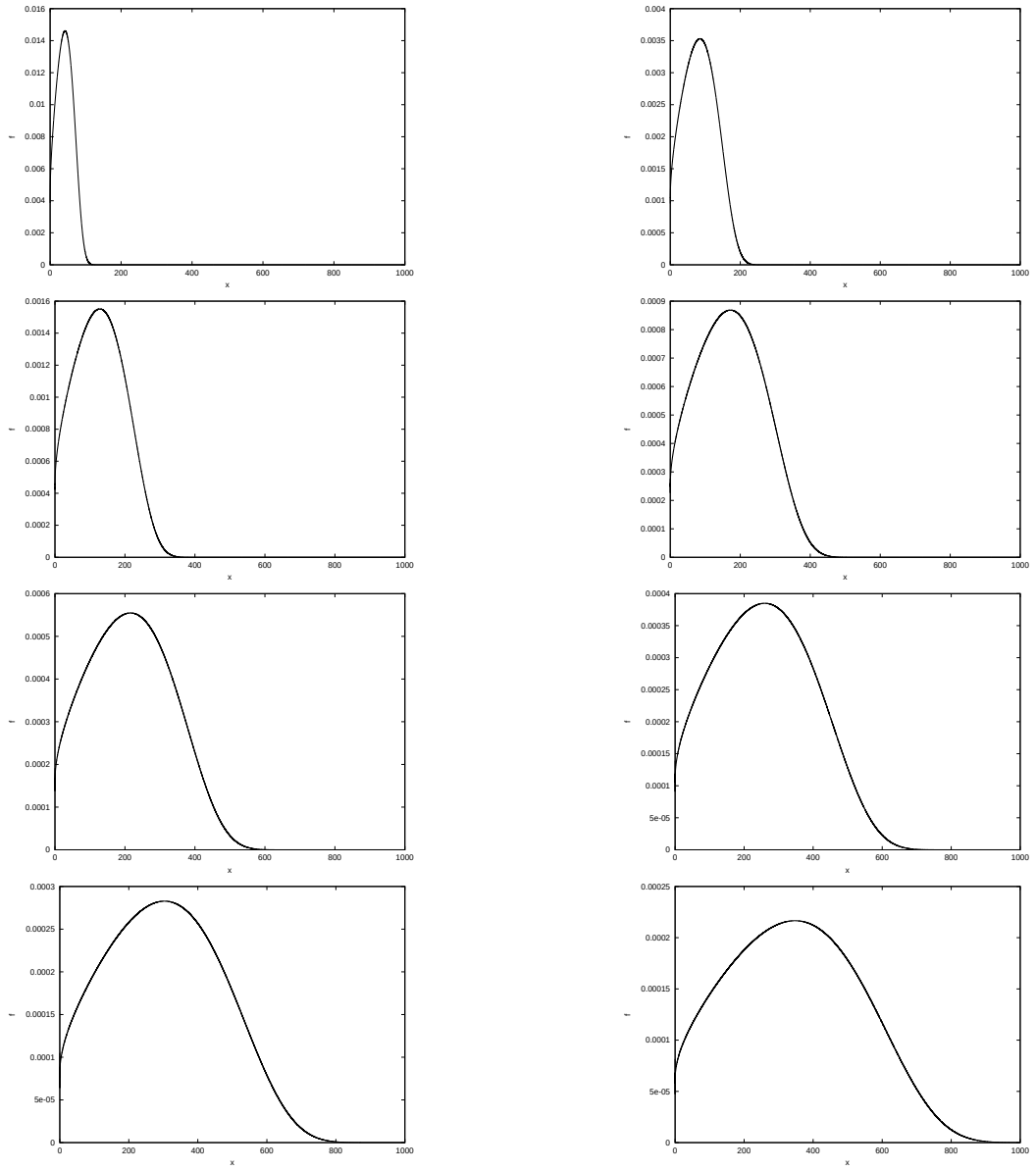

Figure 6: Evolution of the Maxwellian initial data (see Figure 3 bottom right) for the LS system every 250 time units.

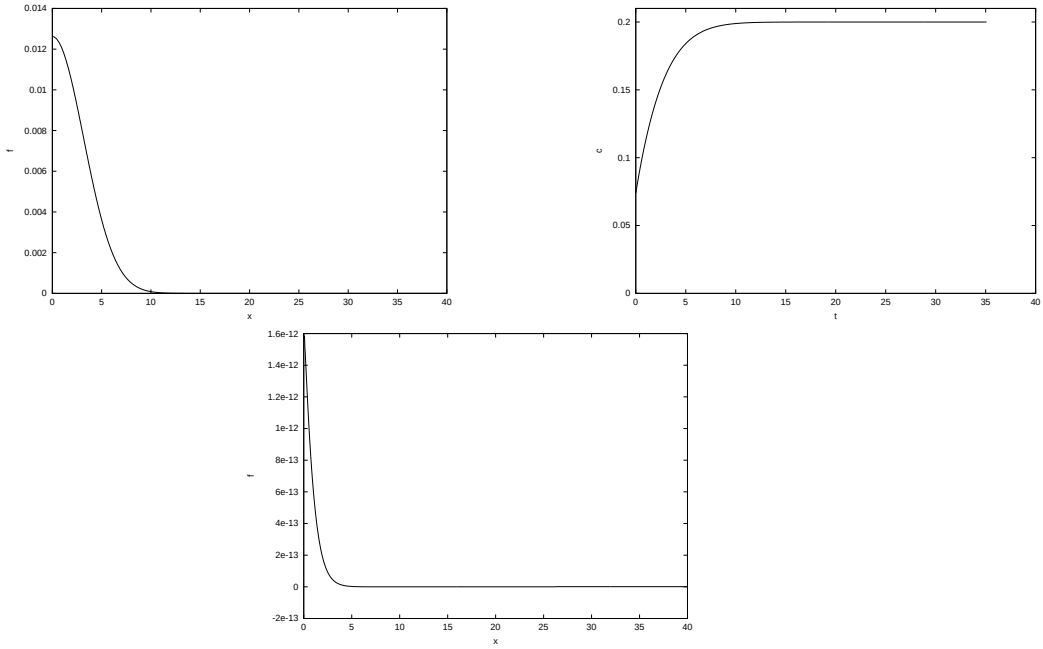

Figure 7: Maxwellian initial data for the LS system ($c(t) \to \rho$): top left: initial data; top right: $c(t)$; bottom: final result.

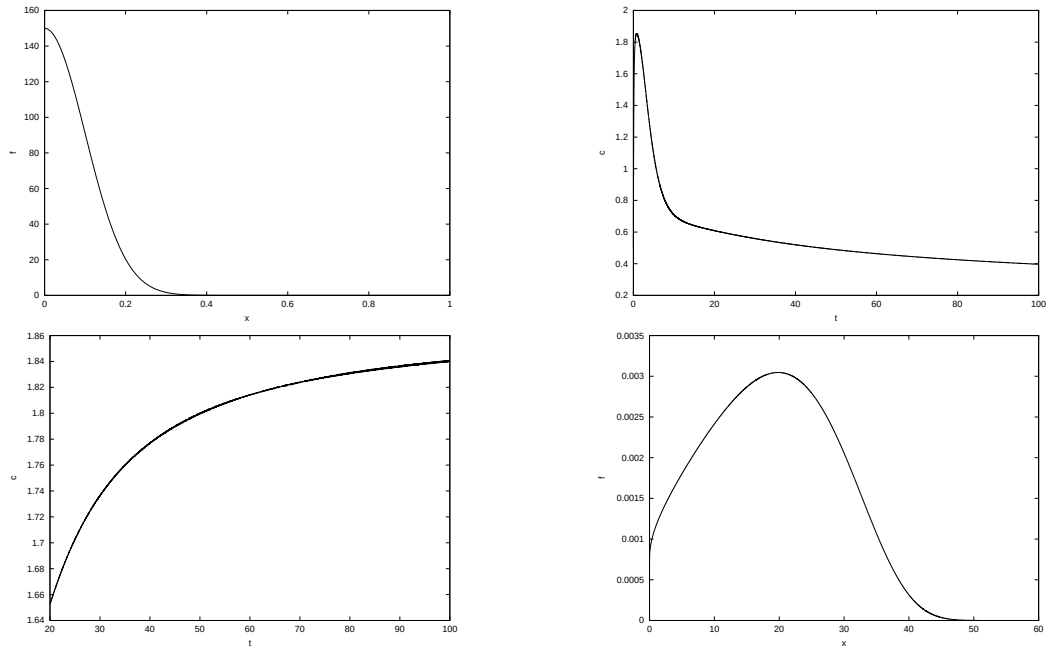

Figure 8: Maxwellian initial data for the LS system ($c(t) \to 0$): top left: initial data; top right: $c(t)$; bottom left: $t^{1/3}c(t)$; bottom right: final result.

Now, we want to check the LS conjecture about the universal asymptotic profile. In order to do this, we take three different initial data (see Figure 9): another smooth non compactly supported initial data: the sum of 2 Maxwellians (we have also tested initial data with unbounded support and algebraic decay); a discontinuous compactly supported initial data: a step function; a continuous non differentiable compactly supported initial data: a triangle function. For which of these initial data we have computed their evolution, the evolution of the concentration of monomers, the evolution of the total number of agglomerates and we have compared the final solution after 2000 units of time with stationary profiles. The results are given in figures 10-11 for the double Maxwellian, 12-13 for the step function and 14-15 for the triangle function.

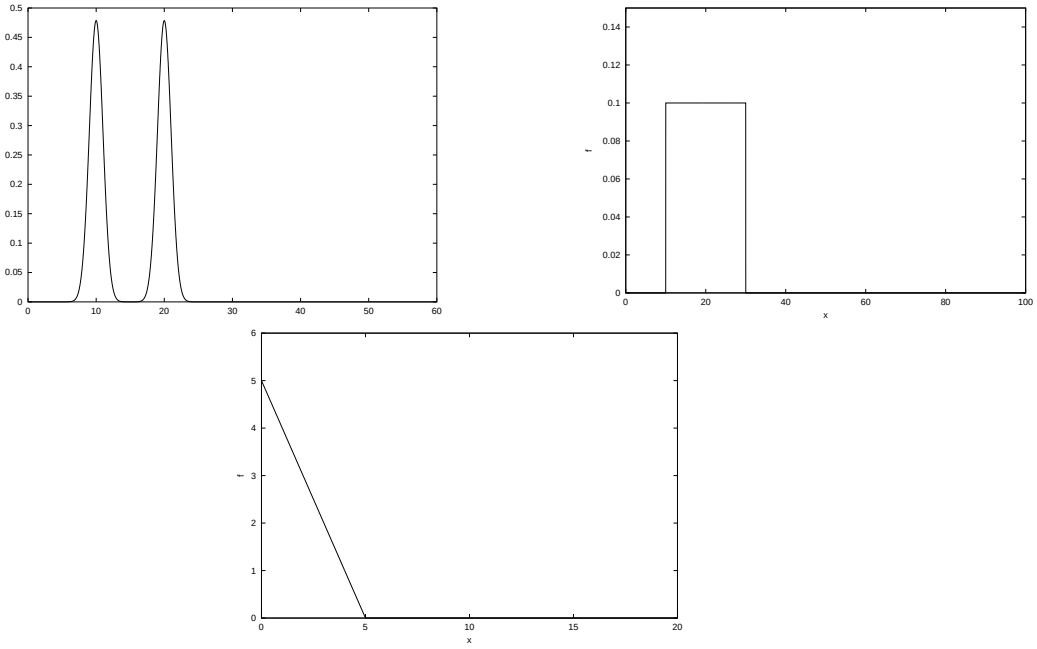

Figure 9: Initial data for the LS system: top left: double Maxwellian; top right: step function; bottom: triangle function.

We conclude from these figures the following observations:

1. A metastability region also appears for the concentration of monomers before $c(t)$ decreases. Note also that in the earlier stages of the evolution, the behaviour of $c(t)$ is much more complicated for the double Maxwellian than for the single one.

2. A good agreement with the $t^{-1/3}$ law, as shown in the graph of $K(t) = t^{1/3}c(t)$. We can observe that the value to which $K(t)$ is converging depends on the initial data. In

fact, for the double Maxwellian we observe values very close to $K_{\text{crit}} = 1.88988$, while for the step function $K(t)$ is larger than this value, it continues to increase and is closer to the value $K = 2.05197$ for $p = 1$ given by (7). Also, for the triangle function $K(t)$ is larger than the critical value $K_{\text{crit}} = 1.88988$, continues to increase and is closer to the value $K = 1.95209$ for $p = 2$ given by (7).

3. m_0 decreases after the metastability region, in good agreement with the t^{-1} law.

4. The evolution of the solutions shows the solution $f(t, x)$ each 250 units of time. We can see clearly the stretching of the support and the convergence towards the shape of the corresponding stationary state given by formula (8).

We have also made tests with functions having unbounded support and algebraic decay at infinity. The conclusions on the behaviour of the solution are the same than those for the Maxwellians and we do not deem necessary to include figures on that case. However, the remarkable point is the great sensitivity of the computation to the necessary truncation of the initial data. We should take under consideration a very large array of initial data, even with very small values in the last components, otherwise the solution could converge to the non smooth prolile associated to the step function. This illustrates once again the high instability of the asymptotic profiles and the high influence of the tail of the initial data.

As a conclusion, we can assert that the conjecture **CLS4** is not verified since the asymptotic profile depends on the initial data while the other conjectures **CLS1**-**CLS3** are numerically satisfied considering non universal constants.

4.2.3 Simulations on the scaled equation

Next, we consider the same set of initial data, but we perform the computations on the rescaled system. As mentioned before, the main advantage is to reduce the size of the domain of computation, since one avoid the stretching of the support of the solution in the new variables.

The price to be paid comes from a considerable increase of the stiffness of the problem, in particular when dealing with the non regular data. This requires to reduce carefuly the CFL condition; otherwise undesirable oscillations can be observed on the computed solutions. These oscillations arise mainly from the end of the support, while d is also oscillating, illustrating again the crucial role played by the largest aggregates. Note that the computational time are comparable to those for the original system, but the rescaled variables are well adapted to go further in time. Let us remind that the variable τ is a logarithmic scale of the variable t.

Results for the Maxwellian and the double Maxwellian can be found in fig. 16-18 and fig. 17-19, respectively. We recover the same conclusions as with the original variables, and the convergence to the expected smooth profile. Let us remark that in this computation we have arrived at $\tau = 25$ and $\tau = 20$, respectively, rescaled time units which correspond to the order of 10^{11} and 10^9 original time units. Therefore, we have gone much further with respect to the simulations in the original system.

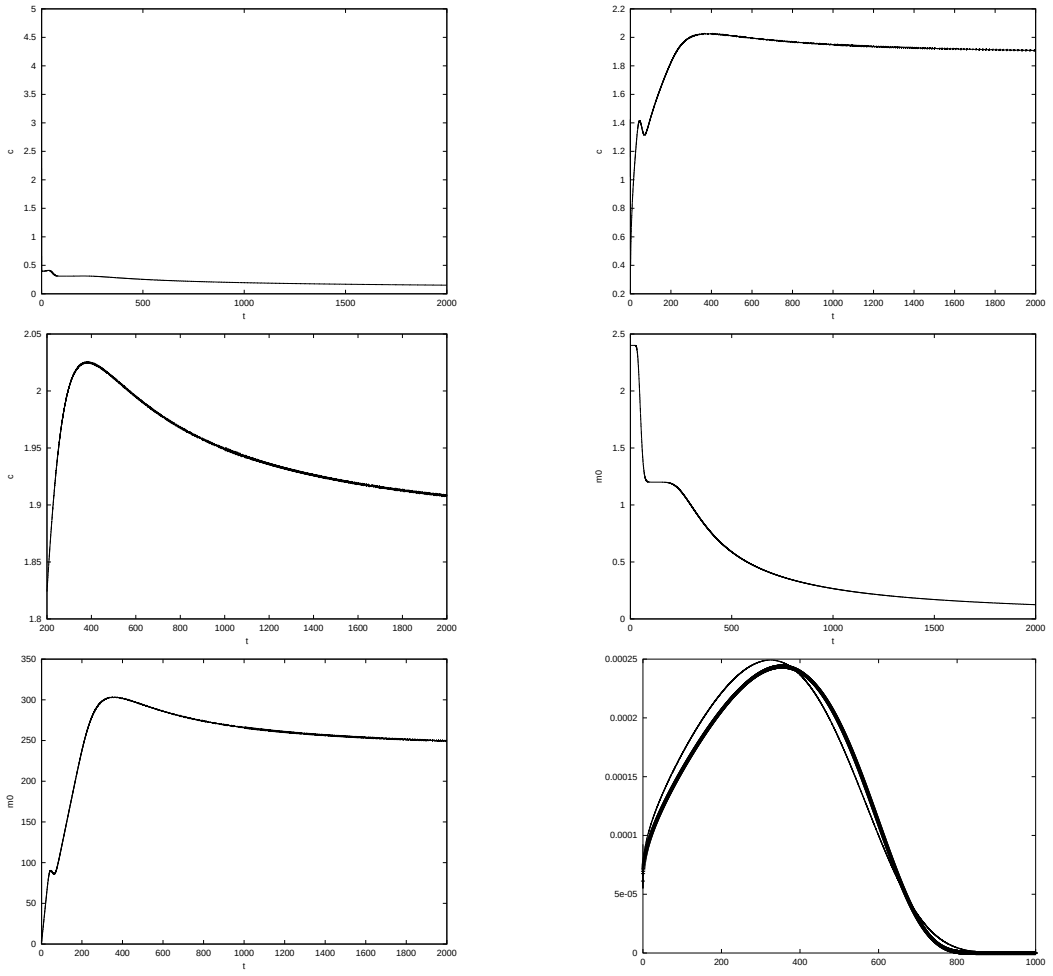

Figure 10: Double Maxwellian initial data for the LS system: top left: $c(t)$; top right: $t^{1/3}c(t)$; middle left: zoom of $t^{1/3}c(t)$; middle right: $m_0(t)$; bottom left: $tm_0(t)$; bottom right: final result (solid line) versus the corresponding LS profile (thicker solid line).

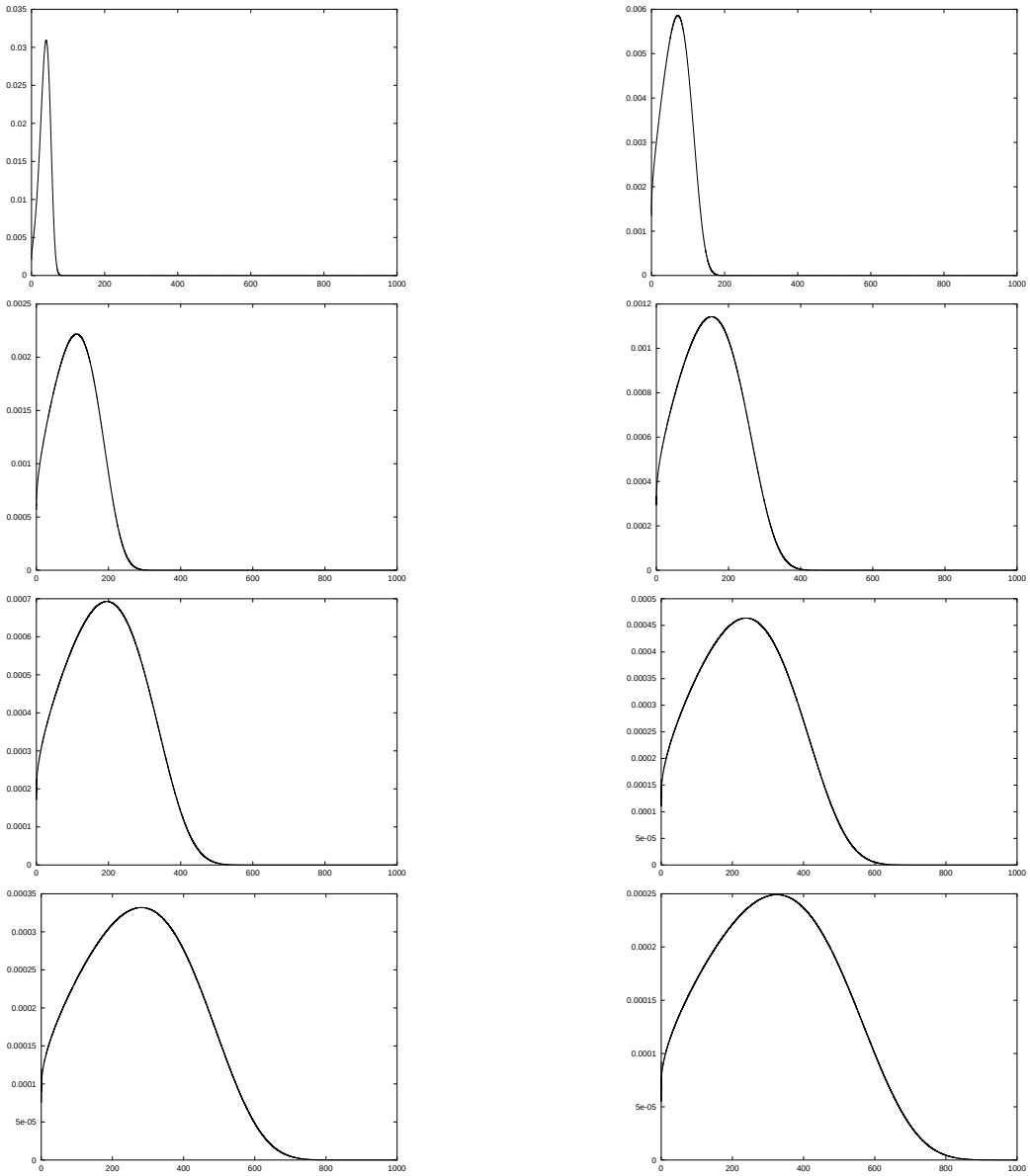

Figure 11: Evolution of the double Maxwellian initial data for the LS system every 250 time units.

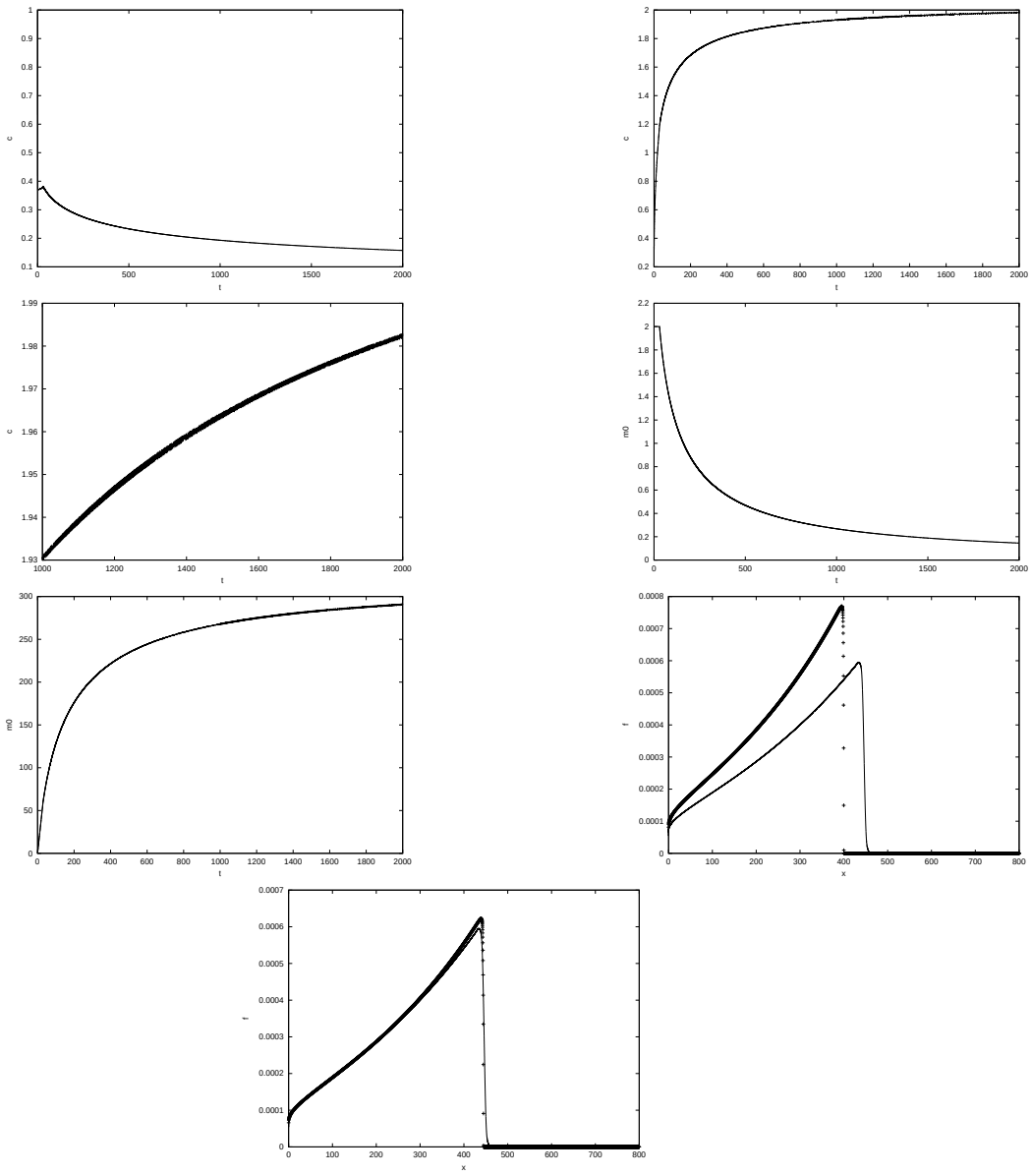

Figure 12: Step function initial data for the LS system: top left: $c(t)$; top right: $t^{1/3}c(t)$; top middle left: zoom of $t^{1/3}c(t)$; top middle right: $m_0(t)$; bottom middle left: $tm_0(t)$; bottom middle right and bottom: final result (solid line) versus the corresponding LS profile (crosses) for two different time delays.

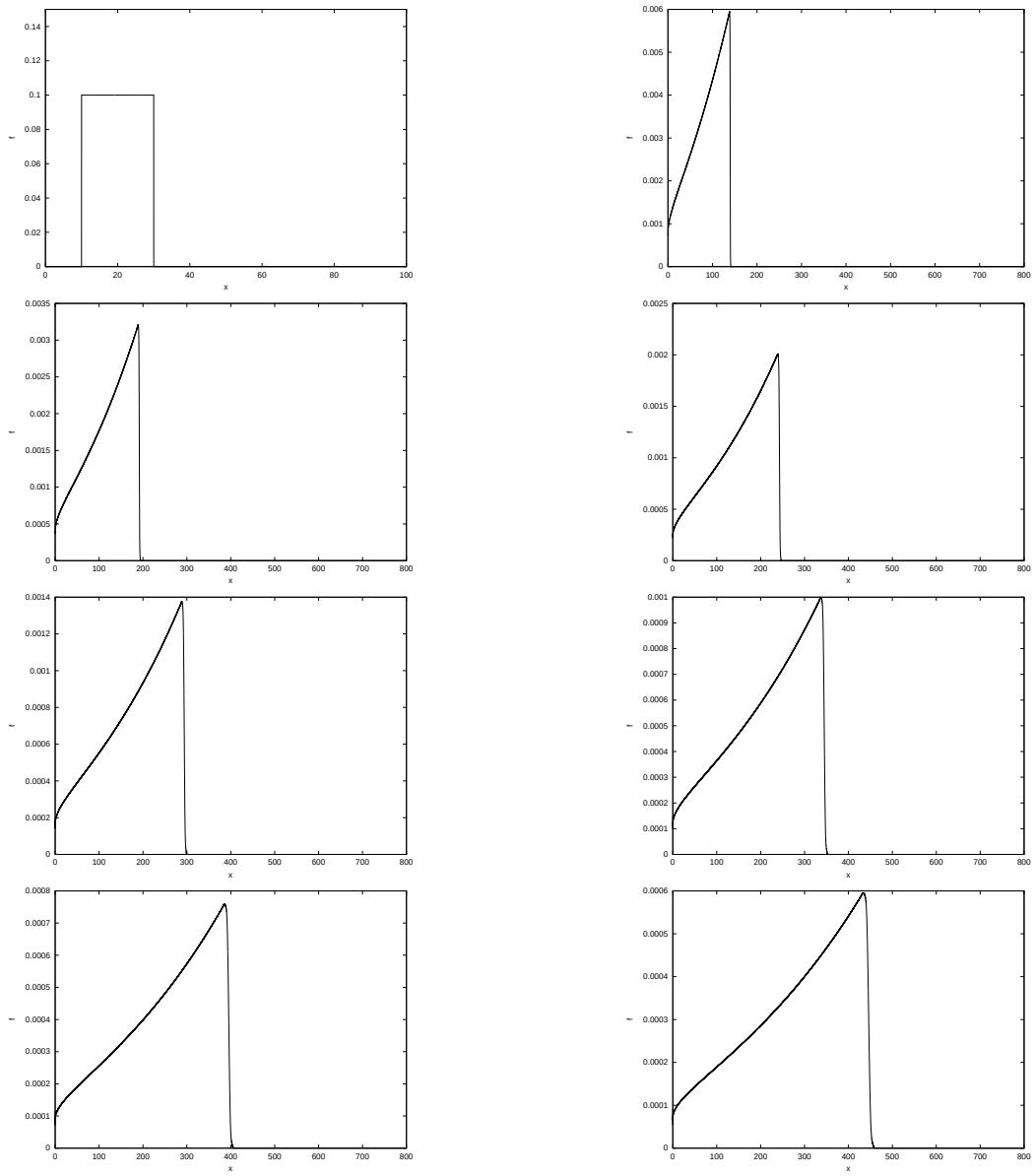

Figure 13: Evolution of the step function initial data for the LS system every 250 time units.

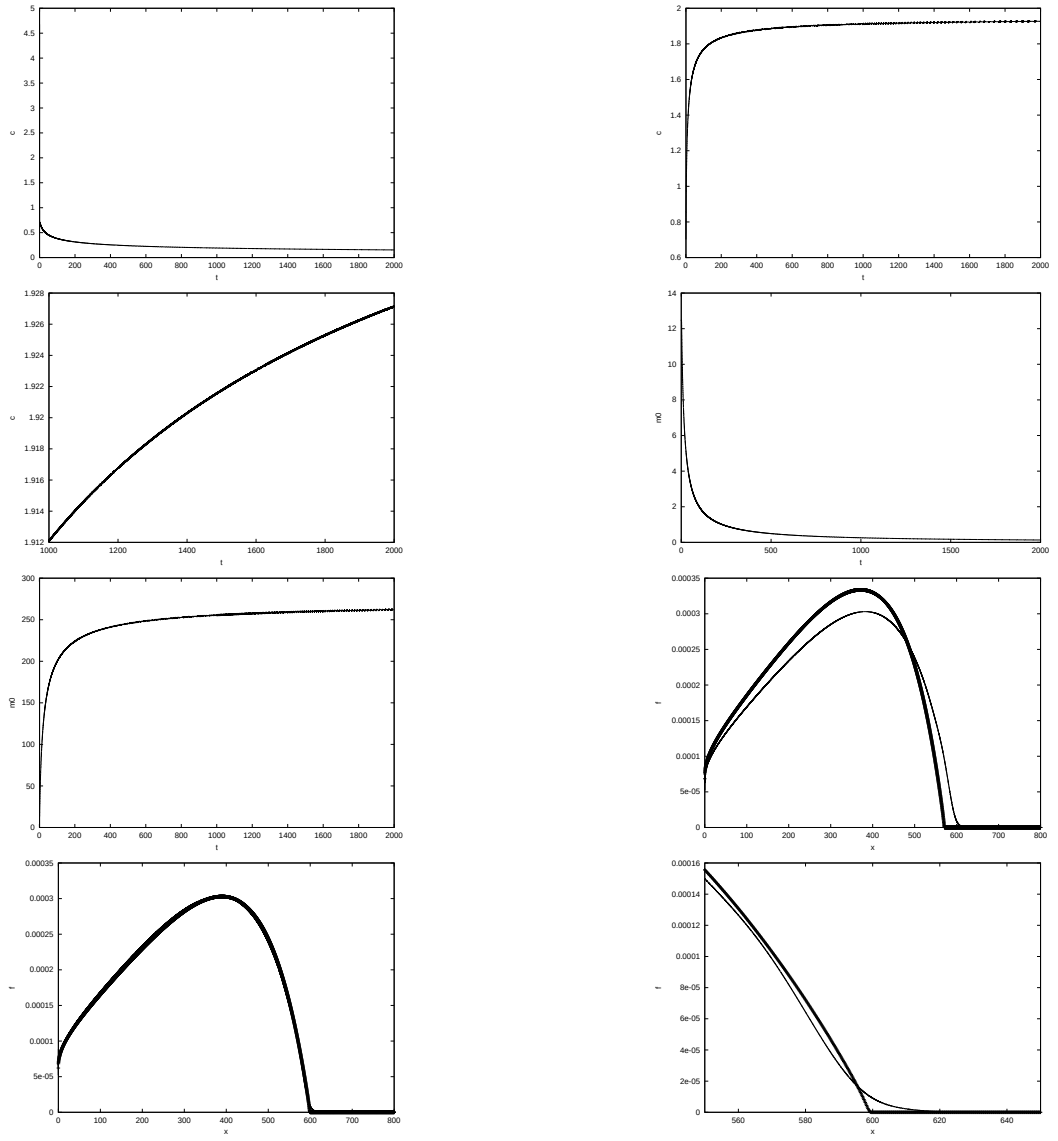

Figure 14: Triangle function initial data for the LS system: top left: $c(t)$; top right: $t^{1/3}c(t)$; top middle left: zoom of $t^{1/3}c(t)$; top middle right: $m_0(t)$; bottom middle left: $tm_0(t)$; bottom middle right and bottom left: final result (solid line) versus the corresponding LS profile (thicker solid line) for two different time delays; bottom right: zoom of the last comparison at the tip of the support.

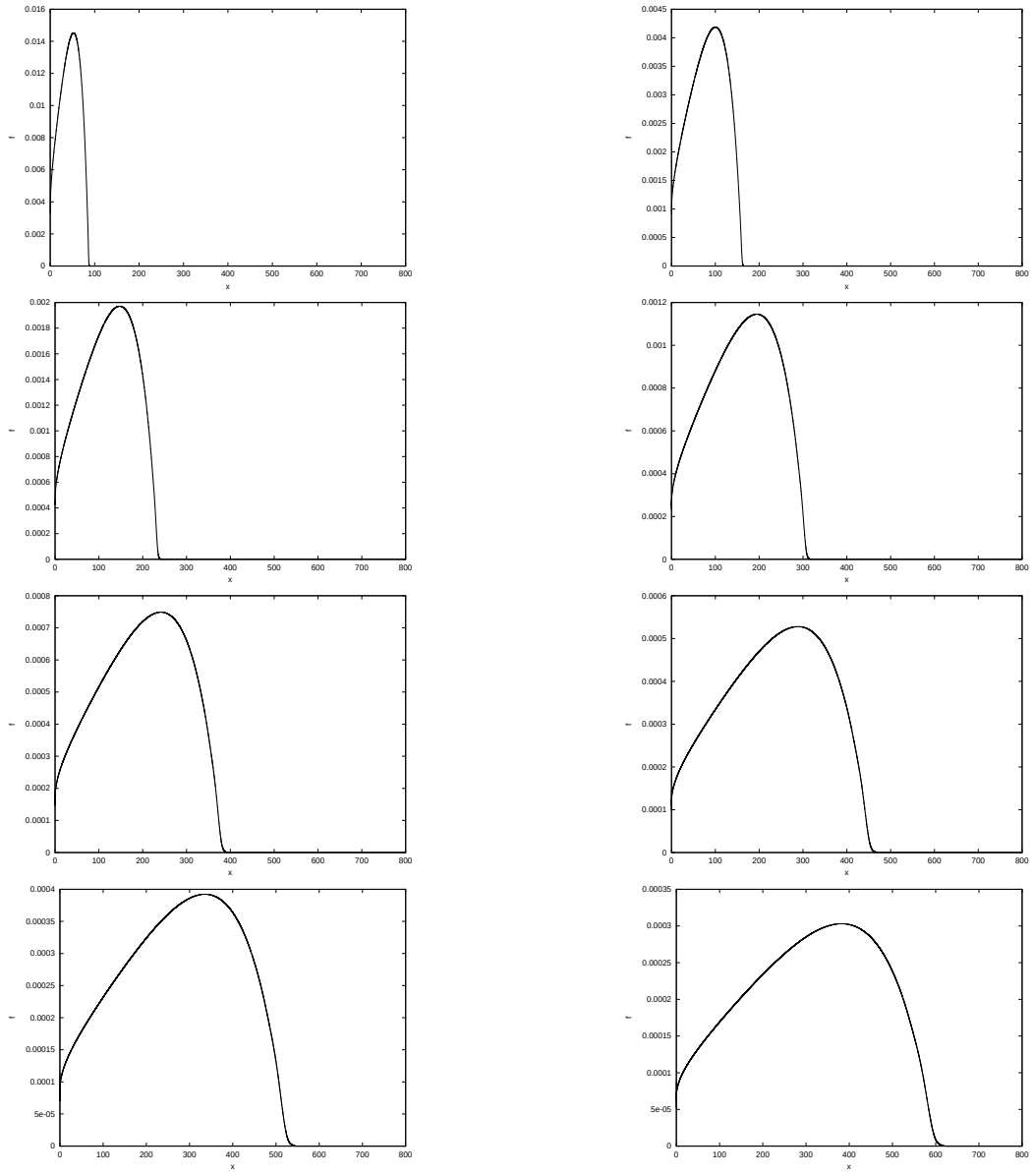

Figure 15: Evolution of the triangle function initial data for the LS system every 250 time units.

Then, fig. 20-21 and fig. 22-23 show the results of the computations for the step function and the triangle as initial data, respectively. Here, we have arrive at $\tau = 10$ rescaled time units which correspond to the order of 10^5 original time units.

Again, one verifies the convergence to the asymptotic profile M_K with the value of K corresponding to the behaviour of the data at the end of its support. However, the problem becomes very stiff as the regularity at the end of the support gets smeared. It should be noted that smearing effects induced by the numerical approximation become noticeable at these very large time for the largest aggregates.

Consequently, while the solution is very close to the profile M_K, it can finally converge to the smooth profile, as illustrated by fig. 20 top, and fig. 23 bottom right. This fact illustrates the enormous numerical difficulty in preserving the precise behaviour of the solution at the tip of the support as time becomes very large, and thus, capturing the right asymptotic profile.

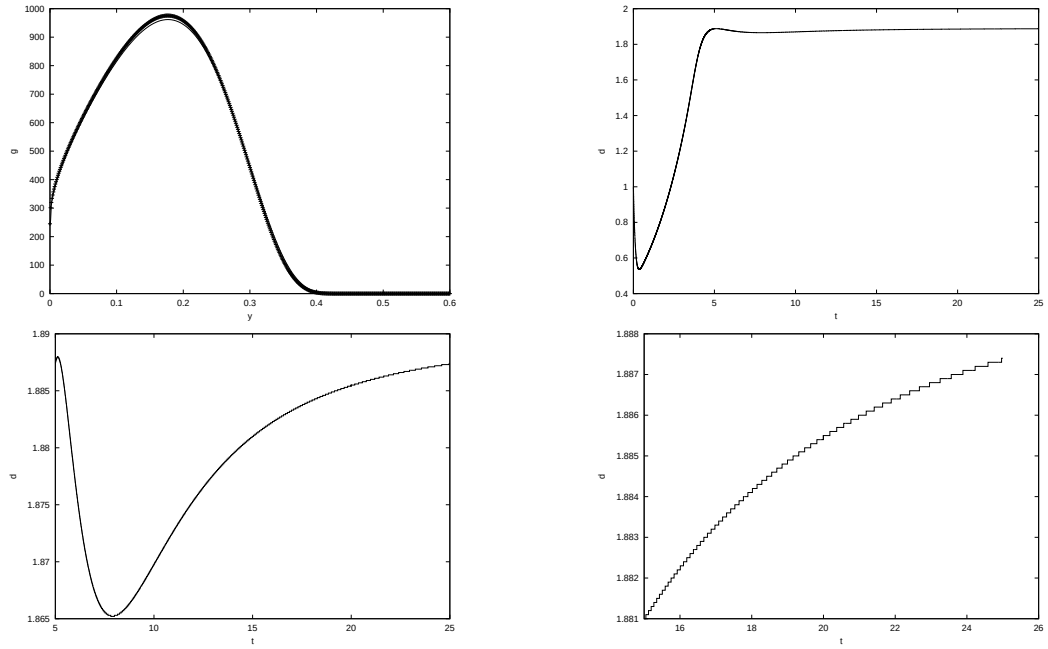

Figure 16: Maxwellian initial data for the rescaled LS system: top left: Comparison between the computed solution after 25 time units (solid line) and the smooth LS profile $M_{\rm crit}$; top right: $d(t)$ is converging towards $K_{\rm crit} = 1.88988$; bottom left and bottom right: zooms of the graph of $d(t)$.

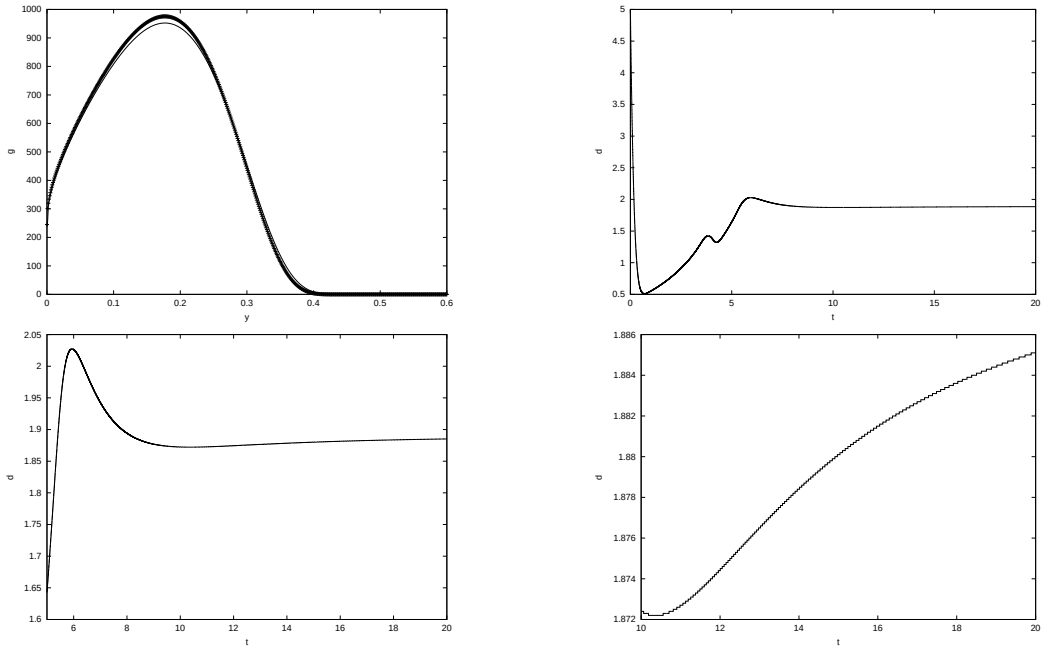

Figure 17: Double Maxwellian initial data for the rescaled LS system: top left: Comparison between the computed solution after 20 time units (solid line) and the smooth LS profile M_{crit}; top right: $d(t)$ is converging towards $K_{\text{crit}} = 1.88988$; bottom left and bottom right: zooms of the graph of $d(t)$.

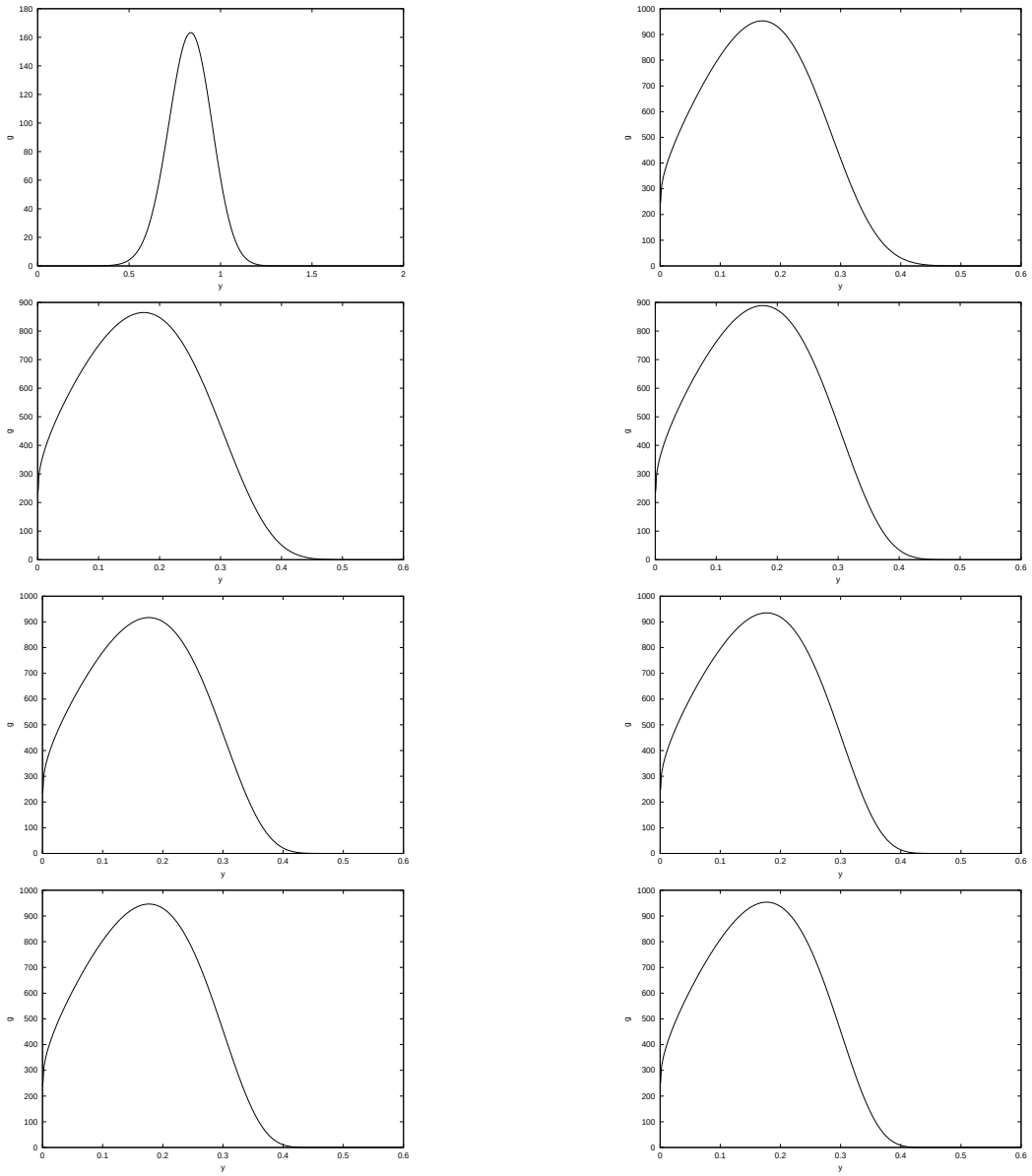

Figure 18: Evolution of the Maxwellian initial data (see Figure 3 bottom right) for the rescaled LS system every 2.5 time units.

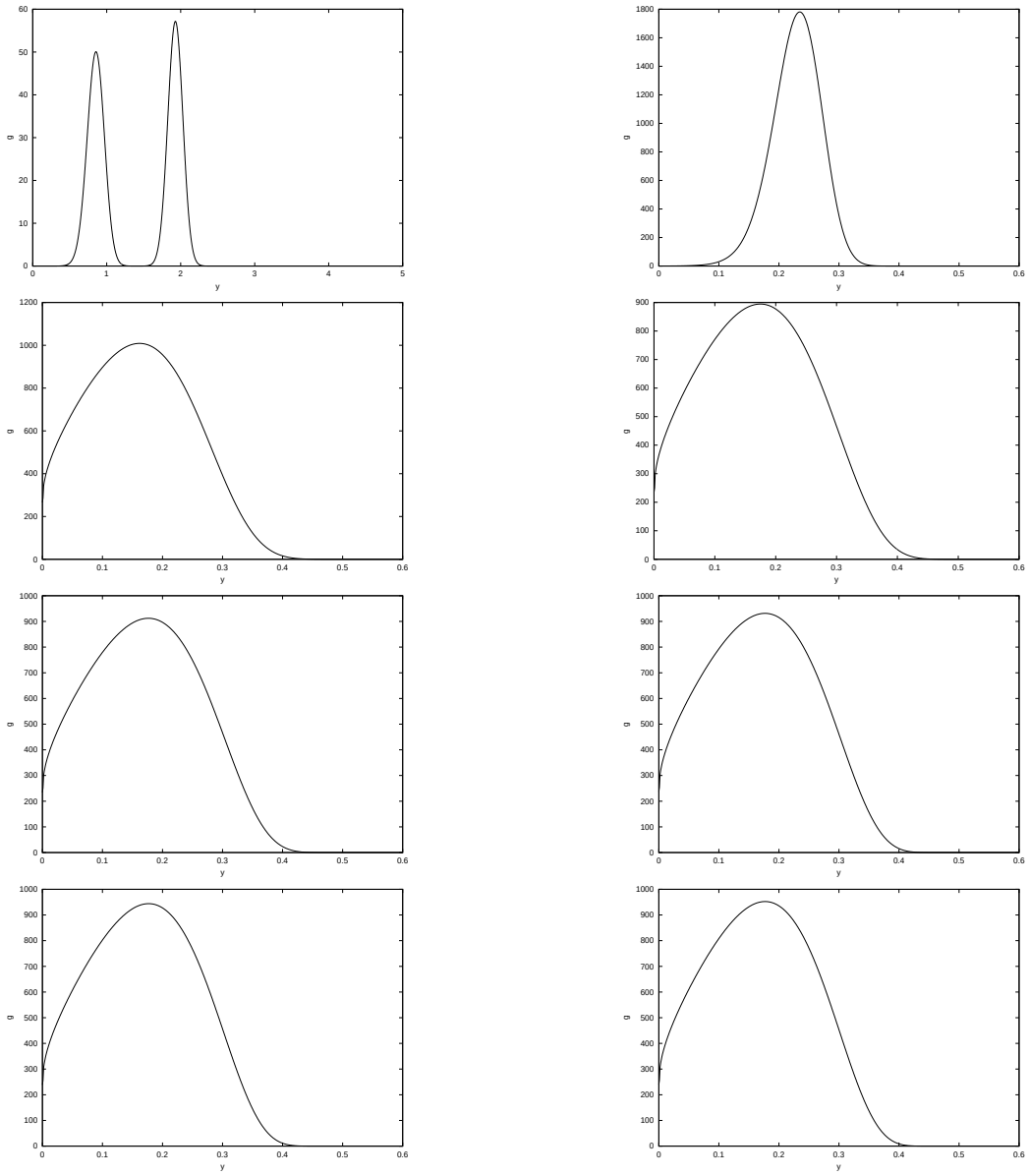

Figure 19: Evolution of the double Maxwellian initial data for the rescaled LS system every 2.5 time units.

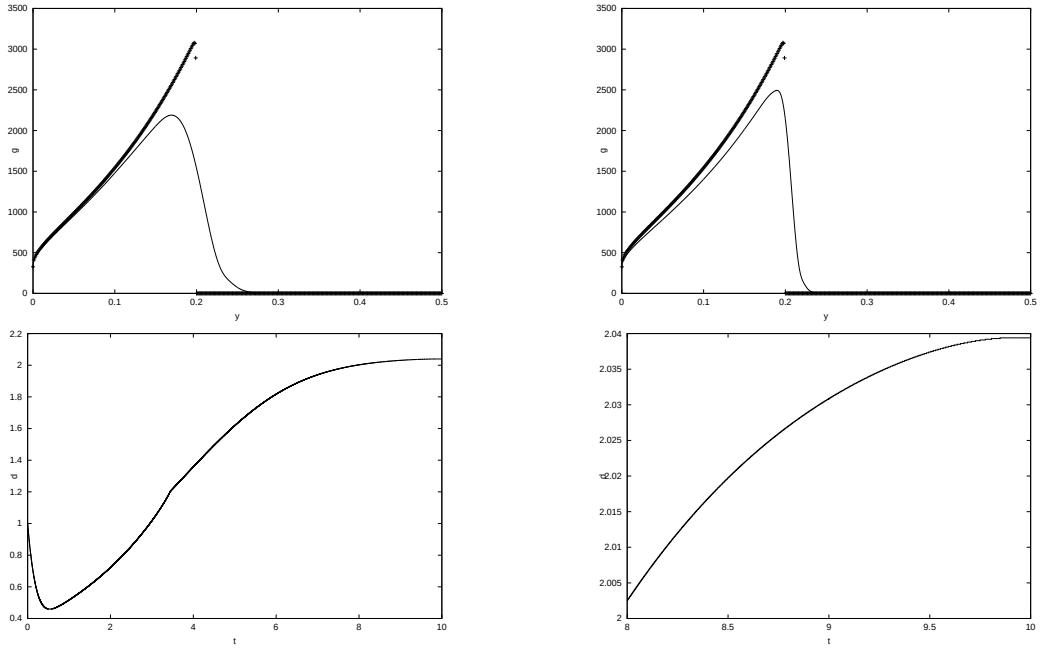

Figure 20: Step function initial data for the rescaled LS system: top left: Comparison between the computed solution after 10 time units (solid line) and the asymptotic profile M_K with $K = 2.05197$; top right: Comparison between the computed solution after 9 time units (solid line) and the asymptotic profile M_K with $K = 2.05197$; bottom left and bottom right: $d(t)$ is converging towards $K = 2.05197$;

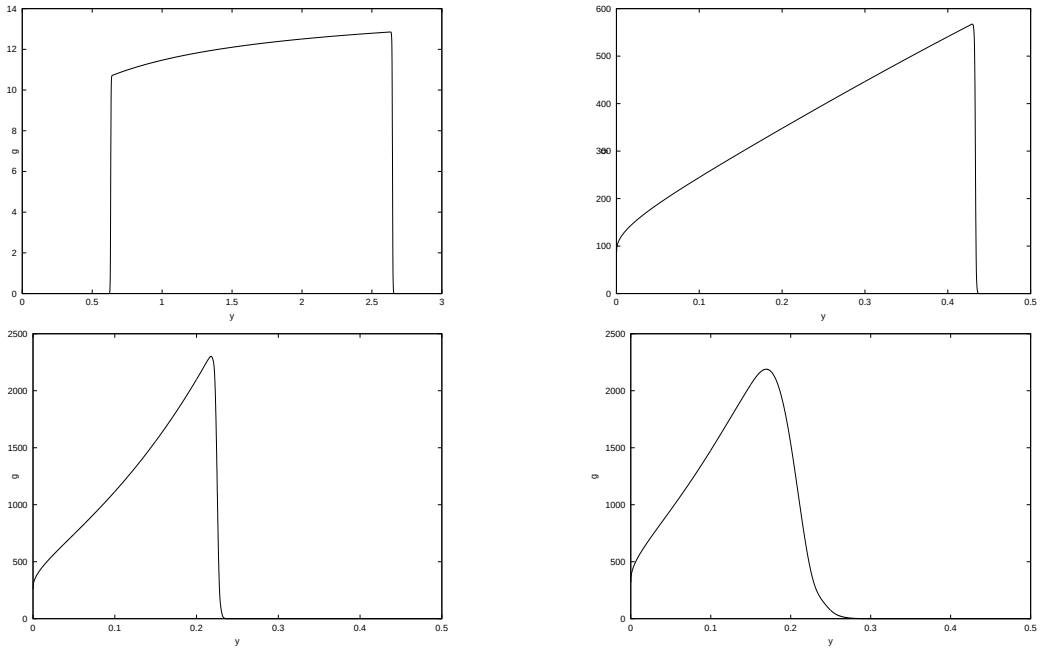

Figure 21: Evolution of the step function initial data for the rescaled LS system every 2.5 time units.

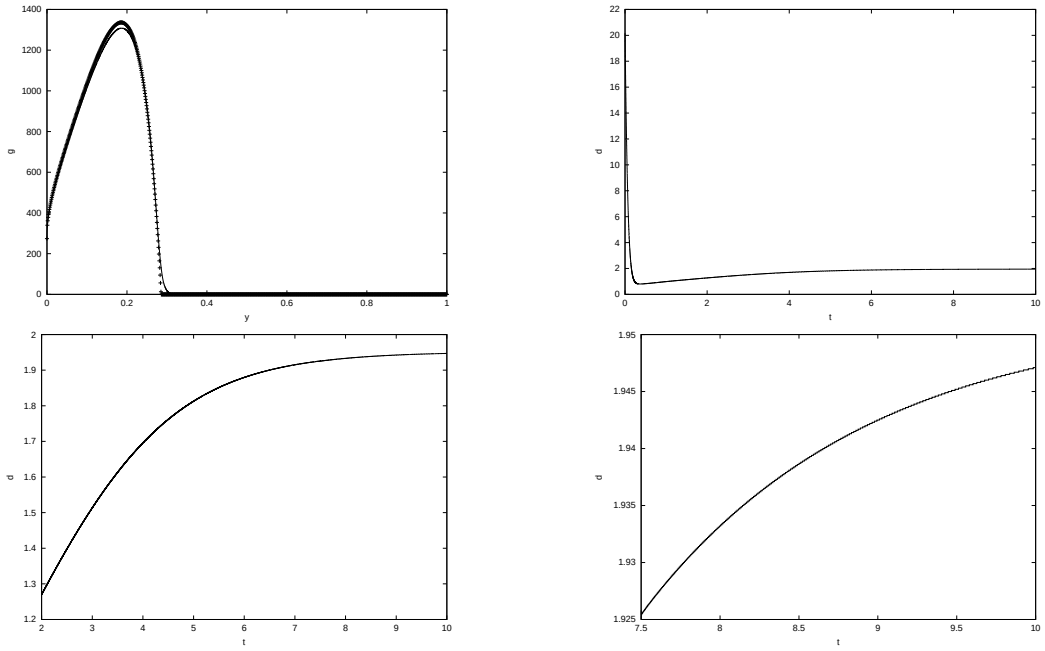

Figure 22: Triangle function initial data for the rescaled LS system: top left: Comparison between the computed solution after 10 time units (solid line) and the asymptotic profile M_K with $K = 1.95209$; top right: $d(t)$ is converging towards $K = 1.95209$; bottom left and bottom right: zooms of the graph of $d(t)$.

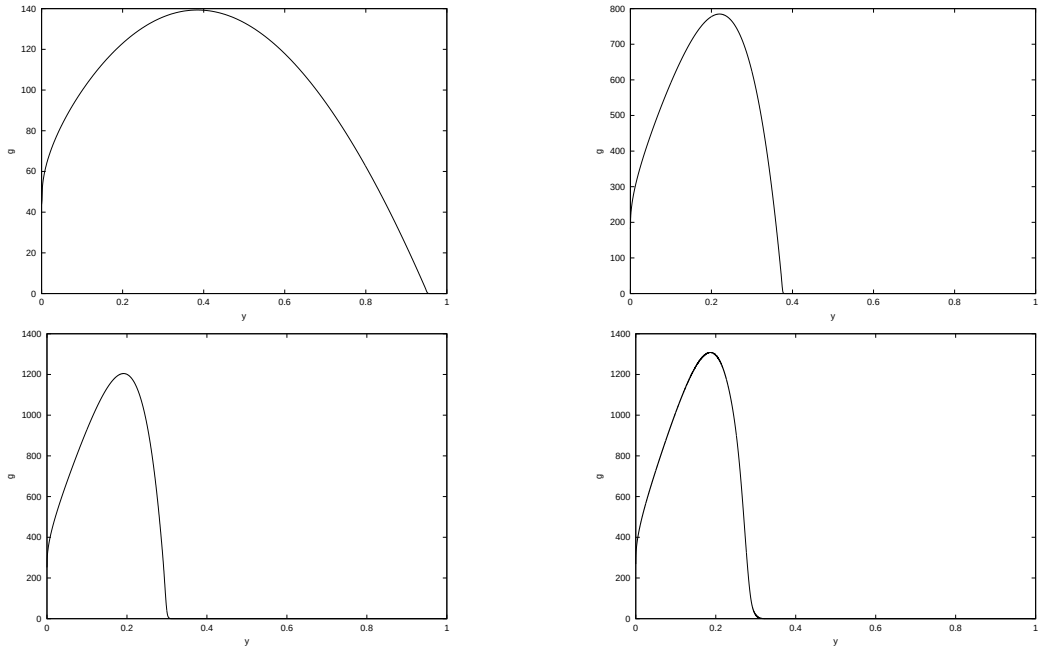

Figure 23: Evolution of the triangle function initial data for the rescaled LS system every 2.5 time units.

4.2.4 Simulations on the LSW equation

Our final tests are devoted to the LSW system. The results showed in fig. 24 and 25 confirm that this system can be seen as a good approximation of the original one for large time, as $c(t)$ has become small, in agreement with the theoretical results in [14]; it also agrees with the prediction proposed in [21] since we recover again the asymptotic profile which corresponds to the behaviour of the initial data at the end of its support.

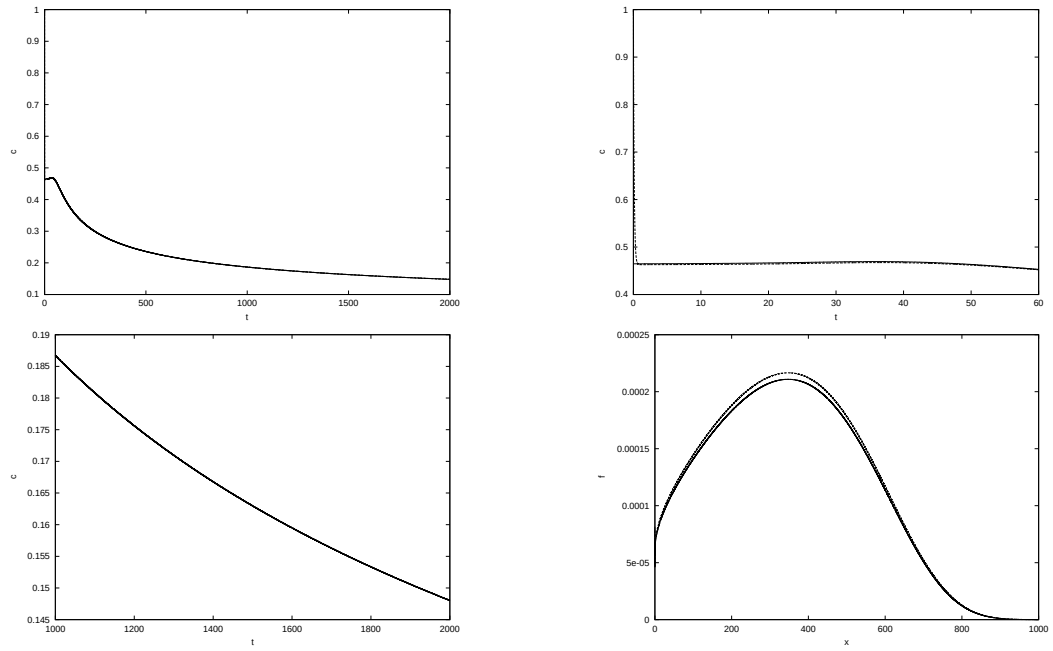

Figure 24: Maxwellian initial data for the LSW system: top right, left and bottom left: Comparison between monomer concentration $c(t)$ for the LS and the LSW; bottom right: Comparison between the computed solutions for the LS and LSW after 2000 time units;

5 Conclusion

The main conclusion of our numerical study is that the asymptotic behaviour of the solutions of the Lifshitz-Slyozov system depends on the initial data. Of course, the challenging question remains to exhibit some condition that guarantee the convergence towards the smooth profile as conjectured in [17]. We expect that our investigation will highlight some elements for finding a solution. First, the convergence to 0 of the monomer concentration certainly does not hold for any initial repartition of mass. Roughly speaking, a certain amount of

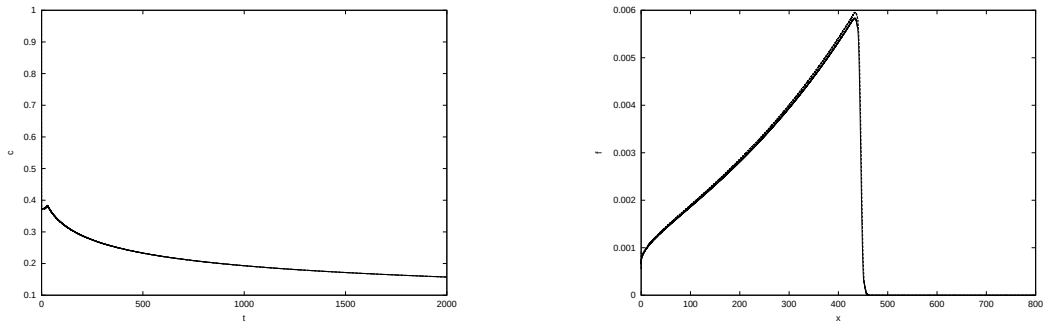

Figure 25: Step initial data for the LSW system: left figure: Comparison between monomer concentration $c(t)$ for the LS and the LSW; right figure: Comparison between the computed solutions for the LS and LSW after 2000 time units;

mass should be given by aggregates larger than the initial critical size. Next, even in situations where $c(t)$ goes to 0, monotonicity is far from clear; in any case it does not concern the earlier stages of evolution where c can have a complicated behaviour.

In our tests, when $c(t) \to 0$, we also verify that $c(t)t^{1/3}$ goes to a constant K. However, the constant depends on the distribution of the largest aggregates present initially in the solution. Accordingly, conjectures **CLS1-CLS3** hold, but with a constant K which depends on the shape of the initial data f_0 and the final profile preserves some memory of the initial shape of the density.

Acknowledgment Partial support from the spanish DGES project PB98-1281 and the TMR Project "Asymptotic Methods in Kinetic Theory", grant number ERB-FRMXCT-970157 are gratefully acknowledged. Part of this work was done while J. A. Carrillo was visiting Labo. J. A. Dieudonné, UMR 6621, University Nice Sophia Antipolis and T. Goudon was visiting the Department of Applied Math., University of Granada. We thank both for their hospitality.

References

[1] Ball J., Carr J., Penrose O., *The Becker-Döring cluster equations: basic properties and asymptotic behaviour of solutions*, Comm. Math. Phys. 104 (1986), no. 4, 657–692.

[2] Becker R., Döring W., *Kinetische behandlung der keimbildung in ubersattigten damfern*, Ann. Phys. (Leipzig), 24, 719-752 (1935).

[3] Brown L., *A new examination of classical coarsening theory*, Acta Metall., 37, 71-77 (1989).

[4] Carr J, Penrose O., *Asymptotic behaviour of solutions to a simplified Lifshitz-Slyozov equation*, Phys. D, 124, 166-176 (1998).

[5] Carrillo J.A., Gamba I.M., Shu C.W., *Computational macroscopic approximations to the 1-D relaxation-time kinetic system for semiconductors*, Physica D, 146, 289-306, (2000).

[6] Chen M., Voorhees P., *The dynamics of transient Ostwald ripening*, Modelling Simul. Mater. Sci. Eng., 1 (1993) 591-612.

[7] Collet J.F., Goudon T., *On solutions of the Lifshitz-Slyozov model*, Nonlinearity, 13, 1239–1262 (2000).

[8] Collet J.F., Goudon T., *Lifshitz-Slyozov equations: the model with encounters*, Transp. Theory Stat. Phys., 28, n. 6, 545-573 (1999)

[9] Collet J.F., Goudon T., Poupaud F., Vasseur A., *The Becker-Döring system and its Lifshitz-Slyozov limit*, Preprint 2000.

[10] Collet J.F., Goudon T., Vasseur A., *Some remarks on the large-time asymptotic of the Lifschitz-Slyozov equations*, Preprint 2001.

[11] Dadyburjor D. B. and Ruckenstein E., *Kinetics of Ostwald ripening*, J. of Crystal Growth, 40, 279-290 (1977).

[12] Jiang G., Shu C.W., *Efficient implementation of weighted ENO schemes*, J. Comp. Physics, 126, 202-228 (1996).

[13] Laurençot P., *Weak solutions to the Lifshitz-Slyozov-Wagner equation*, Preprint 2000.

[14] Laurençot P., *The Lifshitz-Slyozov-Wagner equation with conserved total volume*, Preprint 2001.

[15] Leveque, R.J., *Numerical methods for conservation laws*, Birkhäuser Verlag, 1992.

[16] Lifshitz I.M., Pitaevski L., Cinétique Physique, Coll. Physique Théorique, Landau-Lifshitz (Mir, 1990).

[17] Lifshitz I.M., Slyozov V.V., *The kinetics of precipitation from supersaturated solid solutions*, J. Phys. Chem. Solids, 19, 35-50 (1961).

[18] Meerson B., Sasorov P., *Domain stability, competition, growth, and selection in globally constrained bistable systems*, Phys. Rev. E, 53, 3491-3494 (1996).

[19] Ostwald W., Z. Phys. Chem., 34, 495 (1900).

[20] Niethammer B., Pego R., *On the initial-value problem in the Lifshitz-Slyozov-Wagner theory of Ostwald ripening*, SIAM J. Math. Anal. 31 467-485 (2000).

[21] Niethammer B., Pego R., *Non-self-similar behavior in the LSW theory of Ostwald ripening*, J. Stat. Phys., 95, 867-902 (1999).

[22] Penrose O., *The Becker-Döring equations at large times and their connection with the LSW theory of coarsening*, J. Stat. Phys., 89, 305-320 (1997).

[23] Sagalovich V. V., Slyozov V. V., *Diffusive decomposition of solid solutions*, Sov. Phys. Usp., 30, 23-44 (1987).

[24] Shu C.W., *Essentially Non-oscillatory and weighted essentially non-oscillatory schemes for hyperbolic conservation laws*, NASA/CR-97-206253, ICASE Report 97-65, (1997).

[25] Wagner C., *Theorie der Alterung von Niederschlägen durch Umlösen (Ostwald-Reifung)* Z. Elektrochem. 65, 581-594 (1961).

Contents

Unité de recherche INRIA Sophia Antipolis
2004, route des Lucioles - BP 93 - 06902 Sophia Antipolis Cedex (France)

Unité de recherche INRIA Lorraine : LORIA, Technopôle de Nancy-Brabois - Campus scientifique
615, rue du Jardin Botanique - BP 101 - 54602 Villers-lès-Nancy Cedex (France)
Unité de recherche INRIA Rennes : IRISA, Campus universitaire de Beaulieu - 35042 Rennes Cedex (France)
Unité de recherche INRIA Rhône-Alpes : 655, avenue de l'Europe - 38330 Montbonnot-St-Martin (France)
Unité de recherche INRIA Rocquencourt : Domaine de Voluceau - Rocquencourt - BP 105 - 78153 Le Chesnay Cedex (France)

Éditeur
INRIA - Domaine de Voluceau - Rocquencourt, BP 105 - 78153 Le Chesnay Cedex (France)
http://www.inria.fr
ISSN 0249-6399